석 사 학 위 논 문
Master Thesis

임의 단면을 가진 빔 간의 접촉 거동 모델링

Modeling of contact between beams with arbitrary cross-sections

2017

정 훈 태 (鄭 勳 兌 Jung, Hoontae)

한 국 과 학 기 술 원

Korea Advanced Institute of Science and Technology

석 사 학 위 논 문

임의 단면을 가진 빔 간의
접촉 거동 모델링

2017

정 훈 태

한 국 과 학 기 술 원

기계항공공학부/기계공학과

임의 단면을 가진 빔 간의 접촉 거동 모델링

정 훈 태

위 논문은 한국과학기술원 석사학위논문으로
학위논문 심사위원회의 심사를 통과하였음

2017년 6월 22일

심사위원장 이 필 승 (인)
심 사 위 원 윤 정 환 (인)
심 사 위 원 정 현 (인)

Modeling of contact between beams with arbitrary cross-sections

Jung, Hoontae

Advisor: Lee, Phill-Seung

A thesis submitted to the faculty of
Korea Advanced Institute of Science and Technology in
partial fulfillment of the requirements for the degree of
Master of Science in Mechanical Engineering

Daejeon, Korea
June 22, 2017

Approved by

Lee, Phill-Seung
Professor of Mechanical Engineering

The study was conducted in accordance with Code of Research Ethics[1].

1) Declaration of Ethical Conduct in Research: I, as a graduate student of Korea Advanced Institute of Science and Technology, hereby declare that I have not committed any act that may damage the credibility of my research. This includes, but is not limited to, falsification, thesis written by someone else, distortion of research findings, and plagiarism. I confirm that my dissertation contains honest conclusions based on my own careful research under the guidance of my advisor.

MME
20154549

정훈태. 임의 단면을 가진 빔 간의 접촉 거동 모델링. 기계항공공학부/기계공학과. 2017년. 41+ⅳ 쪽. 지도교수: 이필승. (영문 논문)

Jung, Hoontae. Modeling of contact between beams with arbitrary cross-sections. School of Mechanical and Aerospace Engineering/ Department of Mechanical Engineering. 2017. 41+ⅳ pages. Advisor: Lee, Phill-Seung. (Text in English)

초 록

실제 산업 현장에서 철골 구조물, 케이블 등의 여러 빔 형태의 구조물이 사용되고 있으며, 이에 따라 빔 요소 간의 접촉 현상도 시뮬레이션을 요구하는 경우가 많아지고 있다. 그러나 빔 요소를 이용한 접촉 해석은 주로 원형 단면에 한정되며, 많은 경우 3D 솔리드 모델을 이용할 수 밖에 없다. 본 학위논문에서는 임의의 단면을 가진 빔 요소의 접촉을 해석하는 방법을 제안한다. 이를 위해 임의 단면을 가지는 빔 요소를 해석에 이용하며, 접촉 해석 방법은 점 대 점(point-to-point) 접촉을 개선하여 이용한다. 접촉 거동 모델링의 검증은 기존 논문의 해석 결과 및 상용 프로그램과의 비교를 통하여 이루어졌다.

핵 심 낱 말 유한요소, 접촉, 빔요소, 임의단면 , 점대점접촉

Abstract

Beam structures are used in industrial field included steel structures, cables and so on. Therefore, importance of contact modeling between beams is increasing. However, contact analysis between beams is limited in circular cross-section, so 3D solid elements are used in many beam-to-beam contact cases. In this thesis, the contact modeling between arbitrary cross-sections is suggested by using the beam element with arbitrary cross-sections. The point-to-point contact is modified according to the beam element with arbitrary cross-sections. The validation of contact modeling is performed by reference of existing paper and results of commercial software.

Keywords Finite element, Contact, Beam, Arbitrary cross-section, point-to-point contact

Contents

Contents i

List of Tables ii

List of Figures iii

Chapter 1. Introduction 1

Chapter 2. Continuum Mechanics Based Beam Elements 3
- 2.1 Kinematic of beam elements 3
  - 2.1.1 Interpolation of degenerated elements 3
  - 2.1.2 Kinematics of beam elements for large displacement........ 5
  - 2.1.3 Green-Lagrange strain and total Lagrangian formulation 8

Chapter 3. Beam-to-beam Contact 11
- 3.1 Beam-to-beam contact methods 11
  - 3.1.1 Concept of point-to-point contact 11
  - 3.1.2 Penalty method 12
  - 3.1.3 Formulation of point-to-point contact 14
- 3.2 Improved formulation – non-circular cross-sections 16
  - 3.2.1 Beam-to-beam contact between rectangular cross-section beams 16
  - 3.2.2 Beam-to-beam contact between curbed cross-section beams 17
- 3.3 Improved formulation – multiple contact formulation 19
  - 3.3.1 Concept of line-to-line contact 19

Chapter 4. Contact Algorithm 22
- 4.1 Global and local search 22
- 4.2 Contact determination 25
- 4.3 Contact formulation 29

Chapter 5. Numerical Results 31
- 5.1 Confirmation of difference between 3D beam and 3D solid element 31
- 5.2 Contact between rectangular cross-section beams 32
- 5.3 Contact between beams for four plane elements in cross-section 34
- 5.4 Contact between rectangular hollow beam and square cross-section beam 36

Chapter 6. Conclusions 39

Bibliography 40

List of Tables

Table 5.1 Results of cantilever square beam deflection 31

Table 5.2 Properties of two rectangular cross-section beams 32

Table 5.3 Results of contact between rectangular cross-section beams 33

Table 5.4 Properties of two beams for four plane elements in cross-section 34

Table 5.5 Results of contact between beams for four plane elements in cross-section 35

Table 5.6 Properties of square hollow rectangular beam and square beam 37

Table 5.7 Results of contact between square hollow rectangular beam and square beam 38

List of Figures

Figure 2.1 3D solid finite elements with longitudinal direction and cross-section 3

Figure 2.2 Degenerated beam with beam element and its cross-section 4

Figure 3.1 Kinematics of point-to-point contact 11

Figure 3.2 Diagram of contact situation 12

Figure 3.3 (left) Ideal contact force condition

(right) Contact force using penalty parameter 13

Figure 3.4 A pair of contacting beams with rectangular cross-sections 16

Figure 3.5 Contact search – two closest edges per beam centerline 17

Figure 3.6 Beam-to-beam contact with curved surfaces 17

Figure 3.7 Cross-section and convective coordinate 18

Figure 3.8 Severe inflection, sharped shape (not satisfied C^1-continuous) 19

Figure 3.9 Kinematics of line-to-line contact 19

Figure 3.10 Diagram of line-to-line contact situation 20

Figure 3.11 Different geometrical configurations concerning contact angle and curvature 21

Figure 3.12 Contact of two beams given contact angle α 21

Figure 4.1 Global search – searching between beam nodes 22

Figure 4.2 Difference of closest points with circular and arbitrary cross-section 22

Figure 4.3 Local search – searching between beam edges 23

Figure 4.4 Contact possibility determination – First step 24

Figure 4.5 Contact possibility determination – Second step 24

Figure 4.6 Closest points are checked between every cross-sectional elements 25

Figure 4.7 Contact search of circular cross-section 25

Figure 4.8 Difference of applying contact force on circular and non-circular cross-sections 26

Figure 4.9 Contact search of rectangular cross-section 26

Figure 4.10 Unstable example of edge contact searching 27

Figure 4.11 Contact search of arbitrary cross-section 27

Figure 4.12 Octagonal shape example – this case requires eight condition equations 28

Figure 4.13 A pair of beams and closest edge points 29

Figure 5.1 Cantilever square beam 31

Figure 5.2 Contact between rectangular cross-section beams 32

Figure 5.3 Result of contact between rectangular cross-section beams 33

Figure 5.4 Contact between beams for four plane elements in cross-section 34

Figure 5.5 Results of contact between beams for four plane elements in cross-section 35

Figure 5.6 Contact between square hollow rectangular beam and square beam …………………….......... 36

Figure 5.7 Results of contact between square hollow rectangular beam and square beam 37

Chapter 1. Introduction

Finite element analysis is extensively used in actual field, for example steel frame structures, bridge, construction design, and so on. Beam structures are also included such actual fields, so beam structures occupy important parts in structure analysis. In that case, finite element analysis using beam elements is efficient instead of 3D solid element in terms of cost and time.

In addition, various contact situations are in actual field, for example contact between mechanical elements, contact in manufacturing process, and contact between fibrous materials. In recent years, contact modeling is used in analysis of biopolymer networks. To solve such many contact problems, the finite element analysis is used. The contact problem accompany nonlinear phenomenon as large change of forces and displacements. Therefore, the contact formulations and algorithms have been studied about many finite elements. However, because solid element is universally used, the contact searching algorithms using 2D and 3D solid element were developed quickly such as NTS (Node-to-segment) algorithm [1]. Contact formulation between beams was relatively recently developed.

P. Wriggers and G. Zavarise suggested the contact formulation between three-dimensional beams for the first time [2]. This formulation searches one closest point pair using orthogonality conditions. This beam contact method is called ‘point-to-point’ contact. Most of applied papers about beam-to-beam contact are based point-to-point contact, for example self-contacting on beams experiencing loop formation [3], contact between 3D beams with rectangular cross-sections [4]. Based on point-to-point contact, multiple-point contact between beams was also developed [5-7].

However, the point-to-point contact formulation is developed based on circular cross-section beams. Therefore, P. Litewka suggest the beam-to-beam contact with rectangular cross-sections [4], A. G. neto and P.M. Pimenta suggest the beam-to-beam contact based on smooth curved shape cross-sections, for example superellipses [8]. However, these methods cannot use for arbitrary cross-sections such as I beam, L beam and even arbitrary quadrilateral cross-section. Therefore, simulator have to use solid elements in many beam contact simulations. Most of commercial software also support the beam-to-beam contact between only circular cross-section beams. Because the beam-to-beam contact formulation is developed based circular or limited cross-sections, many applications of beam-to-beam contact are used circular cross-section beams as thin rod, fiber or fabric material, and knot mechanism, or the contact applications irrelevant to shape of cross-section are developed, for example Thermo-electro-mechanical coupling in beam-to-beam contact [16].

In this thesis, the beam-to-beam contact is formulated using the beam with arbitrary cross-sections [7]. This beam element based on continuum mechanics has cross-sectional nodes and 2D shape functions for interpolation of plane node, and cross-sectional plane can be divided multiple elements in cross-section, so very wide variety form of shapes can be made. Using the large displacement analysis for beam contact, the 3D beam element is developed to the nonlinear formulation through large displacement kinematics. Using total Lagrangian formulation, incremental displacements based on the large displacement kinematics are formulated.

Because of using the beam element with non-circular or arbitrary cross-section, the contact algorithm from point-to-point should be modified as applicable to the 3D beam element. In this thesis, the point-to-point contact method and its formulations are introduced. In addition, based on the point-to-point contact method, some improved contact formulations such as change of cross-section or multiple point contact methods are introduced briefly.

Using the 3D degenerated beam element, the new contact searching algorithm and contact formulation are suggested. Through global searching and local searching, closest points on beam surfaces can be found. Then, it is determined whether contact has occurred at the closest points. For determination of contact, new contact determination method is suggested, and modified formulation based on point-to-point contact is introduced. Finally, some numerical examples of beam-to-beam contact for various cross-sections are presented.

Chapter 2. Continuum Mechanics Based Beam Elements

In this chapter, the beam elements to be used in the contact formulations are introduced. Kinematics of beam elements are introduced. Kinematics and formulation of beam elements refer to the reference [15], K. Yoon, *Nonlinear performance of continuum mechanics based beam elements focusing on large twisting behaviors* and the reference [9], K. Yoon, *A continuum mechanics based 3-D beam finite element with warping displacements and its modeling capabilities*.

2.1 Kinematics of beam elements

The beam elements introduced in this chapter are based on degeneration of 3D solid finite elements.

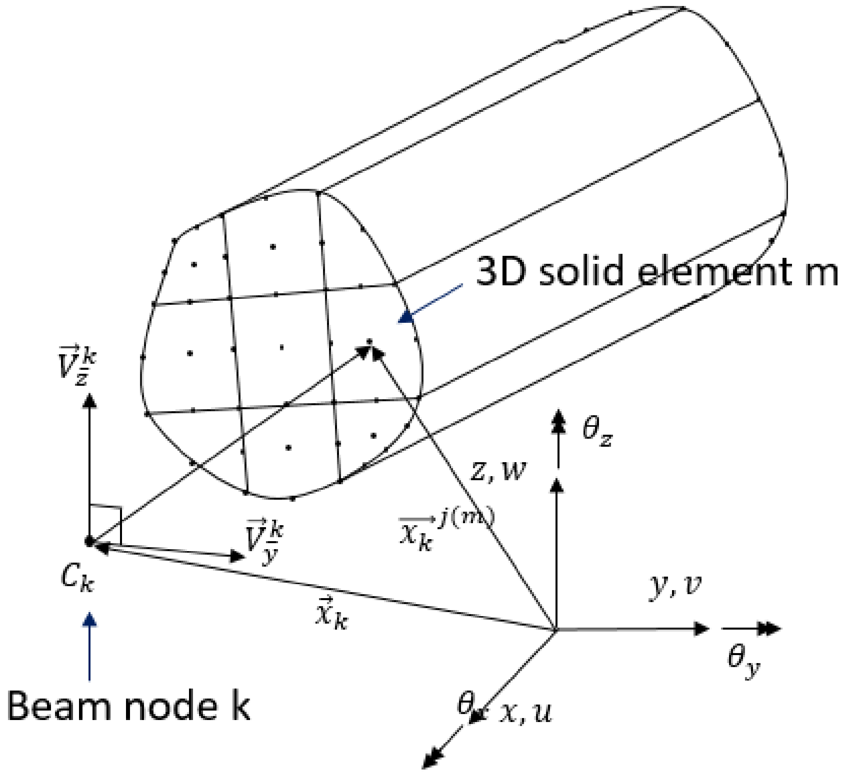

Figure 2.1 3D solid finite elements with longitudinal direction and cross-section

2.1.1. Interpolation of degenerated elements

The beam with arbitrary cross-sections is made by 3D solid elements. The interpolation of the 3D solid element m having n-node is given by

$$\vec{x}^{(m)} = \sum_{i=1}^{n} h_i(r,s,t)\vec{x}_i^{(m)}, \tag{2-1}$$

where $\vec{x}^{(m)}$ is the position in 3D solid element m, and $\overrightarrow{x_i}^{(m)}$ is the position of nodal point i. $h_i(r,s,t)$ is the 3D interpolation function. Through the degeneration of 3D solid beam, $h_i(r,s,t)$ can be divided 1D and 2D interpolation functions, $h_k(r)$ and $h_j(s,t)$. The nodes of 3D solid element are substituted to the plane nodes on the cross-sections of longitudinal direction. So, the degenerated position interpolation is given by

$$\vec{x}^{(m)} = \sum_{i=1}^{q} h_k(r) \sum_{i=1}^{p} h_j(s,t)\, \overrightarrow{x_k}^{j(m)}, \tag{2-2}$$

where $\overrightarrow{x_k}^{j(m)}$ is the vector of plane node j on the cross-section of longitudinal solid element m (See figure 2.1).

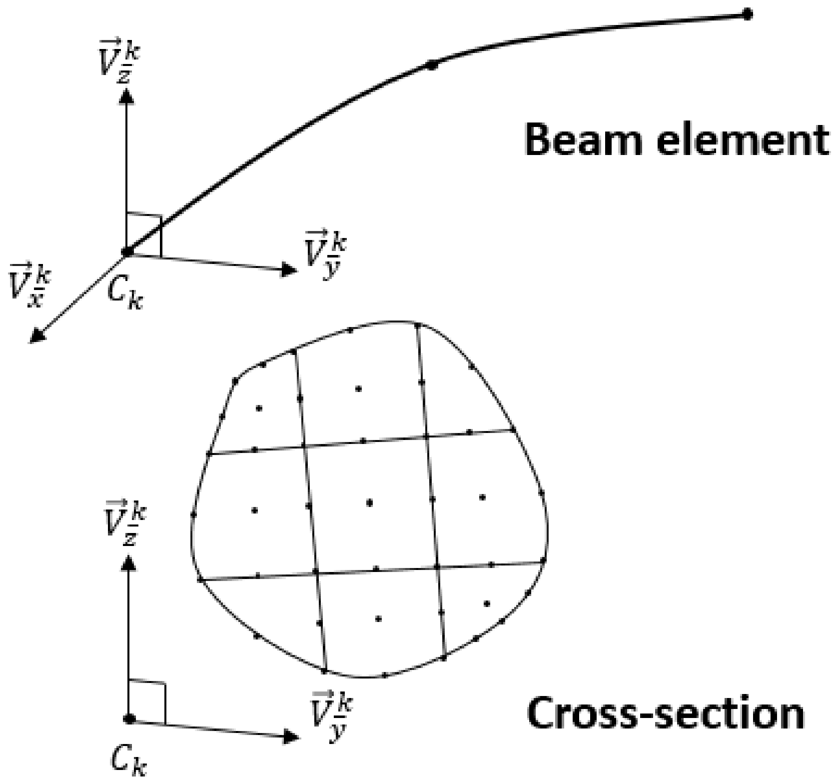

Figure 2.2 Degenerated beam with beam element and its cross-section

Using the beam nodal point and direction vectors on the cross-section as figure 2.2, node $\overrightarrow{x_k}^{j(m)}$ of the solid element can be divided as beam node and cross-sectional node. $\overrightarrow{x_k}^{j(m)}$ is given by

$$\vec{x}_j^{\,j(m)} = \overrightarrow{x_k} + \overrightarrow{y_k}^{j(m)} \overrightarrow{V_{\bar{y}}}^{k} + \overrightarrow{z_k}^{j(m)} \overrightarrow{V_{\bar{z}}}^{k}, \tag{2-3}$$

where $\overrightarrow{y_k}^{j(m)}$ and $\overrightarrow{z_k}^{j(m)}$ are coordinates of nodal point j on the cross-section element of the beam node k, $\overrightarrow{V_{\bar{y}}}^{k}$ and $\overrightarrow{V_{\bar{z}}}^{k}$ are direction vectors on the cross-section of the beam node k. Using (2-2) and (2-3), the equation can be divided the beam node and the cross-sectional node as

$$\vec{x}^{(m)} = \sum_{k=1}^{q} h_k(r)\overrightarrow{x_k} + \sum_{k=1}^{q} h_k(r)\,\bar{y}_k{}^{(m)}\overrightarrow{V_{\bar{y}}}^{k} + \sum_{k=1}^{q} h_k(r)\,\bar{z}_k{}^{(m)}\overrightarrow{V_{\bar{z}}}^{k}, \tag{2-4}$$

where

$$\bar{y}_k{}^{(m)} = \sum_{k=1}^{p} h_j(s,t)\bar{y}_k{}^{j(m)}, \qquad \bar{z}_k{}^{(m)} = \sum_{k=1}^{p} h_j(s,t)\bar{z}_k{}^{j(m)}, \tag{2-5}$$

$\bar{y}_k{}^{(m)}$, $\bar{z}_k{}^{(m)}$ are the cross-sectional positions on beam node *k*. These positions are represented by $\bar{y}_k{}^{j(m)}$, $\bar{z}_k{}^{j(m)}$ as (2-5). $\bar{y}_k{}^{j(m)}, \bar{z}_k{}^{j(m)}$ are nodal point *j* on the cross-section element of beam node *k* in the coordinates of the cross-sectional directions $\overrightarrow{V_{\bar{y}}}^{k}$ and $\overrightarrow{V_{\bar{z}}}^{k}$.

The degenerated beam formulation has 6 degrees of freedom as 3 displacements and 3 rotations. The displacements and rotation angles are defined as u, v, w and $\theta_x, \theta_y, \theta_z$. The rotated directions ${}^{t}\overrightarrow{V_{\bar{y}}}^{k}$ and ${}^{t}\overrightarrow{V_{z}}^{k}$ on the cross-section are represented by rotation angles as

$$\begin{aligned} {}^{t}\overrightarrow{V_{\bar{y}}}^{k} &= \vec{\theta}_k \times \overrightarrow{V_{\bar{y}}}^{k}, \\ {}^{t}\overrightarrow{V_{\bar{z}}}^{k} &= \vec{\theta}_k \times \overrightarrow{V_{\bar{z}}}^{k}, \end{aligned} \tag{2-6}$$

and the normal direction vector of cross-sectional plane is defined as ${}^{t}\overrightarrow{V_{\bar{x}}}^{k} = {}^{t}\overrightarrow{V_{\bar{y}}}^{k} \times \overrightarrow{V_{\bar{z}}}^{k}$,

where $\vec{\theta}_k$ is the rotation angle vector as $\vec{\theta}_k = [\theta_x^k \;\; \theta_y^k \;\; \theta_z^k]$. From equation (2-4) and (2-6), the interpolation of displacements is can derived as

$$\vec{u}^{(m)} = \sum_{k=1}^{q} h_k(r)\overrightarrow{u_k} + \sum_{k=1}^{q} h_k(r)\,\bar{y}_k{}^{(m)}\left(\vec{\theta}_k \times \overrightarrow{V_{\bar{y}}}^{k}\right) + \sum_{k=1}^{q} h_k(r)\,\bar{z}_k{}^{(m)}\left(\vec{\theta}_k \times \overrightarrow{V_{\bar{z}}}^{k}\right), \tag{2-6}$$

Then, the nodal displacement DOFs are $U = [u_k \;\; v_k \;\; w_k \;\; | \;\; \theta_x^k \;\; \theta_y^k \;\; \theta_z^k]$.

2.1.2 Kinematics of beam elements for large displacement

In this section, the nonlinear formulation of the 3D degenerated beam elements for large displacement is introduced. A superscript (or subscript) 0 indicates initial geometry configuration, and *t* indicates current (at time t) configuration. However, *t* does not mean configuration at actual time, but indicates change of configuration. [10]

From equation (2-4), the position vector of the configuration at time *t* is given as

$${}^{t}\vec{x}^{(m)} = \sum_{k=1}^{q} h_k(r)\;{}^{t}\vec{x}_k + \sum_{k=1}^{q} h_k(r)\,\bar{y}_k{}^{(m)}\;{}^{t}\overrightarrow{V_{\bar{y}}}^{k} + \sum_{k=1}^{q} h_k(r)\,\bar{z}_k{}^{(m)}\;{}^{t}\overrightarrow{V_{\bar{z}}}^{k}, \tag{2-7}$$

where ${}^{t}\vec{x}^{(m)}$ is an arbitrary position vector in the beam at time *t*, ${}^{t}\vec{x}_k$ is the position of beam node k at time t, ${}^{t}\overrightarrow{V_{\bar{y}}}^{k}$ and ${}^{t}\overrightarrow{V_{\bar{z}}}^{k}$ are the direction vector on the cross-sectional plane of the beam node *k* at time *t*. At the same element *m*, the incremental displacement is derived from the configuration at time *t* to the configuration at time $t + \Delta t$ as

$$
{}_0\vec{u}^{(m)} = {}^{t+\Delta t}\vec{x}^{(m)} - {}^{t}\vec{x}^{(m)} \quad , \tag{2-8}
$$

Using equation (2-7) and (2-8), the incremental displacement is given as

$$
{}_0\vec{u}^{(m)} = \sum_{k=1}^{q} h_k(r)\, {}_0\vec{u}_k + \sum_{k=1}^{q} h_k(r)\, \bar{y}_k{}^{(m)}\left({}^{t+\Delta t}\overrightarrow{V_{\bar{y}}}^{k} - {}^{t}\overrightarrow{V_{\bar{y}}}^{k}\right) + \sum_{k=1}^{q} h_k(r)\, \bar{z}_k{}^{(m)}\left({}^{t+\Delta t}\overrightarrow{V_{\bar{z}}}^{k} - {}^{t}\overrightarrow{V_{\bar{z}}}^{k}\right) , \tag{2-9}
$$

where ${}_0\vec{u}_k$ is the incremental displacement at the beam node *k* from time t to time $t + \Delta t$. To represent change of director vectors as rotation of director vectors, the Rodrigues rotation formula [11-12] is used as

$$
\mathbf{R}\left({}_0\vec{\theta}^{k}\right) = \mathbf{I} + \frac{\sin\, {}_0\theta^{k}}{{}_0\theta^{k}}\hat{\mathbf{R}}\left({}_0\vec{\theta}^{k}\right) + \frac{1-\cos\, {}_0\theta^{k}}{\left({}_0\theta^{k}\right)^2}\hat{\mathbf{R}}\left({}_0\vec{\theta}^{k}\right)^2, \tag{2-10}
$$

where ${}_0\vec{\theta}^{k} = \left[\, {}_0\theta_x^k \quad {}_0\theta_y^k \quad {}_0\theta_z^k \right]^T, \qquad {}_0\theta^{k} = \sqrt{\left({}_0\theta_x^k\right)^2 + \left({}_0\theta_y^k\right)^2 + \left({}_0\theta_z^k\right)^2}$,

$$
\hat{\mathbf{R}}\left({}_0\vec{\theta}^{k}\right) = \begin{bmatrix} 0 & -\,{}_0\theta_z^k & {}_0\theta_y^k \\ {}_0\theta_z^k & 0 & -\,{}_0\theta_x^k \\ -\,{}_0\theta_y^k & {}_0\theta_x^k & 0 \end{bmatrix} , \tag{2-11}
$$

where ${}_0\theta_x^k,\ {}_0\theta_y^k,\ {}_0\theta_z^k$ are the incremental rotation angles at the beam node *k* from time t to time $t + \Delta t$, and $\hat{R}$ is the antisymmetric matrix by small rotation. It is a matrix form of cross product due to the rotation. Using equation (2-10), the director vectors at time $t + \Delta t$ are represented as

$$
{}^{t+\Delta t}\overrightarrow{V_{\bar{x}}}^{k} = \mathbf{R}\left({}_0\vec{\theta}^{k}\right)\, {}^{t}\overrightarrow{V_{\bar{x}}}^{k},\ {}^{t+\Delta t}\overrightarrow{V_{\bar{y}}}^{k} = \mathbf{R}\left({}_0\vec{\theta}^{k}\right)\, {}^{t}\overrightarrow{V_{\bar{y}}}^{k},\ {}^{t+\Delta t}\overrightarrow{V_{\bar{z}}}^{k} = \mathbf{R}\left({}_0\vec{\theta}^{k}\right)\, {}^{t}\overrightarrow{V_{\bar{z}}}^{k}. \tag{2-12}
$$

Using equation (2-12), the incremental displacement (equation (2-9)) is represented as

$$
{}_0\vec{u}^{(m)} = \sum_{k=1}^{q} h_k(r)\, {}_0\vec{u}_k + \sum_{k=1}^{q} h_k(r)\, \bar{y}_k{}^{(m)}\left(\mathbf{R}\left({}_0\vec{\theta}^{k}\right) - \mathbf{I}\right)\, {}^{t}\overrightarrow{V_{\bar{y}}}^{k} + \sum_{k=1}^{q} h_k(r)\, \bar{z}_k{}^{(m)}\left(\mathbf{R}\left({}_0\vec{\theta}^{k}\right) - \mathbf{I}\right)\, {}^{t}\overrightarrow{V_{\bar{z}}}^{k}, \tag{2-13}
$$

Additionally, the Taylor expansion can be applied in the Rodrigues rotation formula. If apply the Taylor expansion in equation (2-10), the equation can be written as

$$
\mathbf{R}\left({}_0\vec{\theta}^{k}\right) = \mathbf{I} + \hat{\mathbf{R}}\left({}_0\vec{\theta}^{k}\right) + \frac{1}{2!}\hat{\mathbf{R}}\left({}_0\vec{\theta}^{k}\right)^2 + \frac{1}{3!}\hat{\mathbf{R}}\left({}_0\vec{\theta}^{k}\right)^3 + \frac{1}{4!}\hat{\mathbf{R}}\left({}_0\vec{\theta}^{k}\right)^4 + \cdots. \tag{2-14}
$$

In equation (2-14), only linear and quadratic terms are used. Then, equation (2-13) is divided linear terms and extra terms as

$$
{}_0\vec{u}_1^{(m)} = \sum_{k=1}^{q} h_k(r)\, {}_0\vec{u}_k + \sum_{k=1}^{q} h_k(r)\, \bar{y}_k{}^{(m)}\hat{\mathbf{R}}\left({}_0\vec{\theta}^{k}\right)\, {}^{t}\overrightarrow{V_{\bar{y}}}^{k} + \sum_{k=1}^{q} h_k(r)\, \bar{z}_k{}^{(m)}\hat{\mathbf{R}}\left({}_0\vec{\theta}^{k}\right)\, {}^{t}\overrightarrow{V_{\bar{z}}}^{k}, \tag{2-15}
$$

$$
{}_0\vec{u}_2^{(m)} = \frac{1}{2}\sum_{k=1}^{q} h_k(r)\,\bar{y}_k{}^{(m)}\hat{\mathbf{R}}\left({}_0\vec{\theta}^k\right)^2\ {}^t\overrightarrow{V_{\bar{y}}}^k + \frac{1}{2}\sum_{k=1}^{q} h_k(r)\,\bar{z}_k{}^{(m)}\hat{\mathbf{R}}\left({}_0\vec{\theta}^k\right)^2\ {}^t\overrightarrow{V_{\bar{z}}}^k, \tag{2-16}
$$

which ${}_0\vec{u}_1^{(m)}$ and ${}_0\vec{u}_2^{(m)}$ are linear and quadratic terms respectively in the incremental displacement ${}_0\vec{u}^{(m)}$. In the incremental displacement, nodal DOFs vector at beam node k is given as

$$
{}_0U_k = \left[\, {}_0u_k \quad {}_0v_k \quad {}_0w_k \ \mid \ {}_0\theta_x^k \quad {}_0\theta_y^k \quad {}_0\theta_z^k \right]^T, \tag{2-17}
$$

and the total nodal DOFs vector of q beam nodes is given as

$$
{}_0U = \left[\, {}_0U_1^T \quad {}_0U_2^T \quad \cdots \quad {}_0U_q^T \right]^T. \tag{2-18}
$$

Then, ${}_0\vec{u}_1^{(m)}$and ${}_0\vec{u}_2^{(m)}$ are represented in terms of the nodal DOFs vector ${}_0U$ as

$$
{}_0\vec{u}_1^{(m)} = \left[L_1^{(m)} \ \ L_2^{(m)} \ \ \cdots \ \ L_q^{(m)}\right] {}_0U = L^{(m)}\ {}_0U, \tag{2-19}
$$

where

$$
L_k^{(m)} = h_k(r)\left[\mathbf{I} \quad -\left(\bar{y}_k^{(m)}\hat{\mathbf{R}}\left({}^t\overrightarrow{V_{\bar{y}}}^k\right) + \bar{z}_k^{(m)}\hat{\mathbf{R}}\left({}^t\overrightarrow{V_{\bar{z}}}^k\right)\right)\right], \tag{2-20}
$$

and

$$
{}_0\vec{u}_2^{(m)} = \begin{bmatrix} {}_0u_2^{(m)} \\ {}_0v_2^{(m)} \\ {}_0w_2^{(m)} \end{bmatrix} = \frac{1}{2}\begin{bmatrix} {}_0U^T\ {}_1Q^{(m)}\ {}_0U \\ {}_0U^T\ {}_2Q^{(m)}\ {}_0U \\ {}_0U^T\ {}_3Q^{(m)}\ {}_0U \end{bmatrix}, \tag{2-21}
$$

where

$$
{}_iQ^{(m)} = \left[\, {}_iQ_1^{(m)} \quad {}_iQ_2^{(m)} \quad \cdots \quad {}_iQ_q^{(m)}\right], \qquad i = 1,2,3, \tag{2-22}
$$

in which

$$
{}_iQ_k^{(m)} = h_k(r)\begin{bmatrix} \mathbf{0}_{3\times3} & \mathbf{0}_{3\times3} \\ \mathbf{0}_{3\times3} & \bar{y}_k^{(m)}\Psi_i\left({}^t\overrightarrow{V_{\bar{y}}}^k\right) + \bar{z}_k^{(m)}\Psi_i\left({}^t\overrightarrow{V_{\bar{z}}}^k\right) \end{bmatrix}, \tag{2-23}
$$

where

$$
\Psi_1(\vec{x}) = \frac{1}{2}\begin{bmatrix} 0 & x_2 & x_3 \\ x_2 & -2x_1 & 0 \\ x_3 & 0 & -2x_1 \end{bmatrix}, \Psi_2(\vec{x}) = \frac{1}{2}\begin{bmatrix} -2x_2 & x_1 & 0 \\ x_1 & 0 & x_3 \\ 0 & x_3 & -2x_2 \end{bmatrix}, \Psi_3(\vec{x}) = \frac{1}{2}\begin{bmatrix} -2x_3 & 0 & x_1 \\ 0 & -2x_3 & x_2 \\ x_1 & x_2 & 0 \end{bmatrix}. \tag{2-24}
$$

So, variations of the incremental displacements are represented as

$$
\delta\ {}_0\vec{u}_1^{(m)} = L^{(m)}\delta\ {}_0U \ \text{ and } \ \delta\ {}_0\vec{u}_2^{(m)} = \begin{bmatrix} \delta\ {}_0u_2^{(m)} \\ \delta\ {}_0v_2^{(m)} \\ \delta\ {}_0w_2^{(m)} \end{bmatrix} = \begin{bmatrix} \delta\ {}_0U^T\ {}_1Q^{(m)}\ {}_0U \\ \delta\ {}_0U^T\ {}_2Q^{(m)}\ {}_0U \\ \delta\ {}_0U^T\ {}_3Q^{(m)}\ {}_0U \end{bmatrix}. \tag{2-25}
$$

2.1.3 Green-Lagrange strain and total Lagrangian formulation

The covariant Green-Lagrange strain tensor on the beam element *m* in the configuration at time *t* referred to the configuration at time 0 is given as

$$ {}_0^t\varepsilon_{ij}^{(m)} = \frac{1}{2}\left({}^t\mathbf{g}_i^{(m)} \cdot {}^t\mathbf{g}_j^{(m)} - {}^0\mathbf{g}_i^{(m)} \cdot {}^0\mathbf{g}_j^{(m)} \right) \ , i,j = 1,2,3 \tag{2-26} $$

where ${}^t\mathbf{g}_i^{(m)}$ is the covariant basis of convective system (*r*,*s*,*t*), and it is given as

$$ {}^t\mathbf{g}_i^{(m)} = \frac{\partial\ {}^t x^{(m)}}{\partial r_i}, i,j = 1,2,3 \tag{2-27} $$

Because the cross-sectional deformations are not existed in Timoshenko beam theory, the strain tensors are considered about only 5 components as ${}_0^t\varepsilon_{11}^{(m)}, {}_0^t\varepsilon_{12}^{(m)}, {}_0^t\varepsilon_{21}^{(m)}, {}_0^t\varepsilon_{13}^{(m)}, {}_0^t\varepsilon_{31}^{(m)}$, and other 4 components as ${}_0^t\varepsilon_{22}^{(m)}, {}_0^t\varepsilon_{23}^{(m)}, {}_0^t\varepsilon_{32}^{(m)}, {}_0^t\varepsilon_{33}^{(m)}$ are zeros.

The local Green-Lagrange strain tensor ${}_0^t\bar{\varepsilon}_{ij}^{(m)}$ in the local Cartesian coordinate system has following relationship with the covariant Green-Lagrange strain tensor ${}_0^t\varepsilon_{ij}^{(m)}$,

$$ {}_0^t\bar{\varepsilon}_{ij}^{(m)}\left({}^0t_i \otimes {}^0t_j \right) = {}_0^t\varepsilon_{kl}^{(m)}\left({}^0\mathbf{g}^{k(m)} \otimes {}^0\mathbf{g}^{l(m)} \right), \tag{2-28} $$

where the base vectors in the local Cartesian coordinate system are given by

$$ {}^0t_1 = h_k(r)\ {}^0V_{\bar{x}}^k,\ {}^0t_2 = h_k(r)\ {}^0V_{\bar{y}}^k,\ {}^0t_3 = h_k(r)\ {}^0V_{\bar{z}}^k, \tag{2-29} $$

and, ${}^0\mathbf{g}^{i(m)}$ is the contravariant basis vectors, and there are have following relationship as

$$ {}^0\mathbf{g}^{i(m)} \cdot {}^0\mathbf{g}_j^{(m)} = \delta_j^i \ , \tag{2-30} $$

in which δ_j^i is the Kronecker delta, it means $\delta_j^i = 1$ if $i = j$,and $\delta_j^i = 0$ if $i \neq j$.

Using equation (2-26), the incremental covariant Green-Lagrange strain on the beam element *m* is represented as

$$ {}_0\varepsilon_{ij}^{(m)} = {}_0^{t+\Delta t}\varepsilon_{ij}^{(m)} - {}_0^t\varepsilon_{ij}^{(m)} = \frac{1}{2}\left({}^t\mathbf{g}_i^{(m)} \cdot {}_0\vec{u}_{,j}^{(m)} + {}^t\mathbf{g}_j^{(m)} \cdot {}_0\vec{u}_{,i}^{(m)} + {}_0\vec{u}_{,i}^{(m)} \cdot {}_0\vec{u}_{,j}^{(m)} \right) \tag{2-31} $$

where ${}_0\vec{u}_{,i}^{(m)} = \frac{\partial\ {}_0\vec{u}^{(m)}}{\partial r_i}$.

Using ${}_0\vec{u}^{(m)} \approx {}_0\vec{u}_1{}^{(m)} + {}_0\vec{u}_2{}^{(m)}$, equation (2-31) can be divided linear term and nonlinear term as

$$ {}_0\varepsilon_{ij}^{(m)} \approx {}_0e_{ij}^{(m)} + {}_0\eta_{ij}^{(m)} + {}_0\kappa_{ij}^{(m)} \ , \tag{2-32} $$

where ${}_0e_{ij}^{(m)}$ is linear term and ${}_0\eta_{ij}^{(m)}$ is nonlinear term by the linear incremental displacement ${}_0\vec{u}_1{}^{(m)}$, and ${}_0\kappa_{ij}^{(m)}$ is nonlinear term by the quadratic incremental displacement ${}_0\vec{u}_2{}^{(m)}$ as follows,

$$ {}_0e_{ij}^{(m)} = \tfrac{1}{2}\left({}^t\mathbf{g}_i^{(m)} \cdot {}_0\vec{u}_{1,j}^{(m)} + {}^t\mathbf{g}_j^{(m)} \cdot {}_0\vec{u}_{1,i}^{(m)} \right),\ {}_0\eta_{ij}^{(m)} = \tfrac{1}{2}\left({}_0\vec{u}_{1,i}^{(m)} \cdot {}_0\vec{u}_{1,j}^{(m)} \right), $$

$$ {}_0\kappa_{ij}^{(m)} = \frac{1}{2}\left({}^t\mathbf{g}_i^{(m)} \cdot {}_0\vec{u}_{2,j}^{(m)} + {}^t\mathbf{g}_j^{(m)} \cdot {}_0\vec{u}_{2,i}^{(m)} \right) \tag{2-33} $$

Using equation (2-19) and (2-21), the relations between incremental Green-Lagrange strain and incremental nodal DOFs are obtained as

$$
\begin{aligned}
{}_0e_{ij}^{(m)} &= \frac{1}{2}\left({}^t\mathbf{g}_i^{(m)} \cdot L_{,j}^{(m)} + {}^t\mathbf{g}_j^{(m)} \cdot L_{,i}^{(m)} \right) {}_0U = B_{ij}^{(m)}\ {}_0U, \\
{}_0\eta_{ij}^{(m)} &= \frac{1}{2}\ {}_0U^T \left(L_{,i}^{(m)T} L_{,j}^{(m)} \right) {}_0U = \frac{1}{2}\ {}_0U^T\ {}_1N_{ij}^{(m)}\ {}_0U, \\
{}_0\kappa_{ij}^{(m)} &= \frac{1}{2}\ {}_0U^T \left({}^t\mathbf{g}_i^{(m)} \cdot \hat{Q}_{,j}^{(m)} + {}^t\mathbf{g}_j^{(m)} \cdot \hat{Q}_{,i}^{(m)} \right) {}_0U = \frac{1}{2}\ {}_0U^T\ {}_2N_{ij}^{(m)}\ {}_0U,
\end{aligned} \tag{2-34}
$$

where $L_{,i}^{(m)} = \frac{\partial L^{(m)}}{\partial r_i}$ and $\hat{Q}_{,i}^{(m)} = \left[\frac{\partial\ {}_1Q^{(m)}}{\partial r_i} \quad \frac{\partial\ {}_2Q^{(m)}}{\partial r_i} \quad \frac{\partial\ {}_3Q^{(m)}}{\partial r_i} \right]^T$.

Using equation (2-28), the incremental covariant Green-Lagrange strains are changed to the local Green-Lagrange strains as

$$
\begin{aligned}
{}_0\bar{e}_{ij}^{(m)} &= B_{ij}^{(m)} \left(t_i \cdot \mathbf{g}^{k(m)} \right) \left(t_j \cdot \mathbf{g}^{l(m)} \right) {}_0U = \bar{B}_{ij}^{(m)}\ {}_0U, \\
{}_0\bar{\eta}_{ij}^{(m)} &= \frac{1}{2}\ {}_0U^T\ {}_1N_{ij}^{(m)} \left(t_i \cdot \mathbf{g}^{k(m)} \right) \left(t_j \cdot \mathbf{g}^{l(m)} \right) {}_0U = \frac{1}{2}\ {}_0U^T\ {}_1\bar{N}_{ij}^{(m)}\ {}_0U, \\
{}_0\bar{\kappa}_{ij}^{(m)} &= \frac{1}{2}\ {}_0U^T\ {}_2N_{ij}^{(m)} \left(t_i \cdot \mathbf{g}^{k(m)} \right) \left(t_j \cdot \mathbf{g}^{l(m)} \right) {}_0U = \frac{1}{2}\ {}_0U^T\ {}_2\bar{N}_{ij}^{(m)}\ {}_0U,
\end{aligned} \tag{2-35}
$$

The equilibrium equation in nonlinear analysis is obtained to the principal virtual work at time $t + \Delta t$, and the configuration at time t is known. Through the principal virtual work, the equilibrium equation is represented to the incremental equation, that process is called total Lagrangian formulation. From the total Lagrangian formulation, the equilibrium equation consists of three parts, tangential stiffness matrix, force vector and internal force. [10]

The total Lagrangian formulation is given by

$$
\int_{{}^0V} \delta\ {}_0\bar{e}_{ij}\ \bar{C}_{ijrs}\ {}_0\bar{e}_{rs} d\ {}^0V + \int_{{}^0V} {}_0^t\bar{S}_{ij} \delta\ {}_0\bar{\eta}_{ij}\ d\ {}^0V + \int_{{}^0V} {}_0^t\bar{S}_{ij} \delta\ {}_0\bar{\kappa}_{ij}\ d\ {}^0V = {}^{t+\Delta t}\mathbf{R} - \int_{{}^0V} {}_0^t\bar{S}_{ij} \delta\ {}_0\bar{e}_{ij}\ d\ {}^0V, \tag{2-36}
$$

where ${}^0V$ is the volume of beam element at time 0, ${}^{t+\Delta t}\mathbf{R}$ is the external virtual work, $\bar{C}_{ijrs}$ is the material law in local Cartesian coordinate and ${}_0^t\bar{S}_{ij}$ is the second Piola-Kirchhoff stress in local Cartesian coordinate. Because the strain tensor has only 5 non-zero components as (i,j) are (1,1), (1,2), (2,1), (1,3) and (3,1), the material law tensor also has only 5 non-zero components as $\bar{C}_{1111} = E, \bar{C}_{1212} = \bar{C}_{2121} = \bar{C}_{1313} = \bar{C}_{3131} = G$, where E is Young's modulus and G is shear modulus.

Using equation (2-35), equation (2-36) can be discretized as

$$
\begin{aligned}
&\delta\ {}_0U^T \left[\sum_{m=1}^{n} \int_{{}^0V^{(m)}} \bar{B}_{ij}^{(m)T} \bar{C}_{ijrs} \bar{B}_{rs}^{(m)} dV^{(m)} + \sum_{m=1}^{n} \int_{{}^0V^{(m)}}\ {}_1\bar{N}_{ij}^{(m)}\ {}_0^t\bar{S}_{ij} dV^{(m)} + \sum_{m=1}^{n} \int_{{}^0V^{(m)}}\ {}_2\bar{N}_{ij}^{(m)}\ {}_0^t\bar{S}_{ij} dV^{(m)} \right] {}_0U \\
&= \delta\ {}_0U^{T\ t+\Delta t}R - \delta\ {}_0U^T \left[\sum_{m=1}^{n} \int_{{}^0V^{(m)}} \bar{B}_{ij}^{(m)T}\ {}_0^t\bar{S}_{ij} dV^{(m)} \right],
\end{aligned} \tag{2-37}
$$

where *n* is total number of the beam elements, ${}^0V^{(m)}$ is the volume of beam element m at time 0.

Equation (2-37) can be simplified as follows

$$({}^{t}K_{L} + {}^{t}K_{N1} + {}^{t}K_{N2})\, {}_{0}U = {}^{t+\Delta t}R - {}_{0}^{t}F \tag{2-38}$$

where

$$\begin{aligned}
{}^{t}K_{L} &= \sum_{m=1}^{n} \int_{{}^{0}V^{(m)}} \bar{B}_{ij}^{(m)T} \bar{C}_{ijrs} \bar{B}_{rs}^{(m)} dV^{(m)} \quad , \\
{}^{t}K_{N1} &= \sum_{m=1}^{n} \int_{{}^{0}V^{(m)}} {}_{1}\bar{N}_{ij}^{(m)}\, {}_{0}^{t}\bar{S}_{ij} dV^{(m)} \quad , \\
{}^{t}K_{N2} &= \sum_{m=1}^{n} \int_{{}^{0}V^{(m)}} {}_{2}\bar{N}_{ij}^{(m)}\, {}_{0}^{t}\bar{S}_{ij} dV^{(m)} \quad , \\
{}_{0}^{t}F &= \sum_{m=1}^{n} \int_{{}^{0}V^{(m)}} \bar{B}_{ij}^{(m)T}\, {}_{0}^{t}\bar{S}_{ij} dV^{(m)} \quad .
\end{aligned} \tag{2-39}$$

Finally, we can obtain the incremental displacement ${}_{0}U$ through equation (2-38).

Chapter 3. Beam-to-beam Contact

In this chapter, the existing beam-to-beam contact methods will be introduced. The contact method in the thesis is motivated by point-to-point contact method, so the contact formulation of point-to-point will be explained. The concept of penalty method used in point-to-point contact is also explained. In addition, improved contact formulations based on point-to-point contact are introduced.

3.1 Beam-to-beam contact methods

P. Wriggers and G. Zavarise suggest the beam-to-beam contact formulation between three-dimensional beams at first in 1997 [2]. This formulation has two features, the beam is circular cross-section and the contact points is one pair in minimum distance between the beams. This formulation is called to 'Point-to-point' contact. Many beam-to-beam contact formulations are improved by based the point-to-point contact formulation. Improved formulations revise the two features, for example, the cross-sections are changed, or the contact points are changed. The point-to-point contact and the improved formulations are introduced briefly.

3.1.1 Concept of point-to-point contact

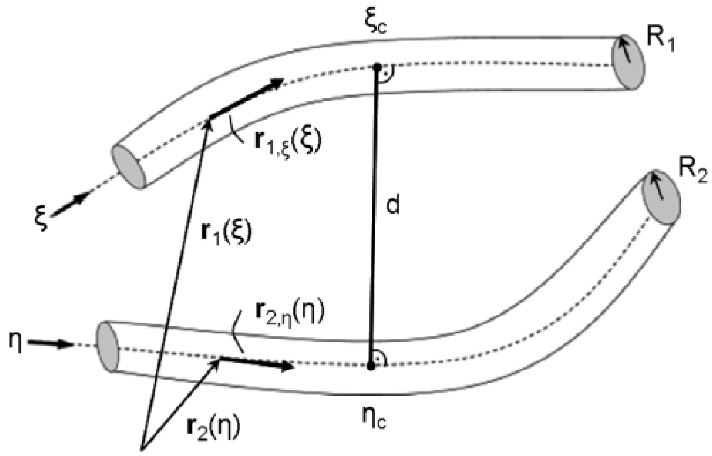

Figure 3.1 Kinematics of point-to-point contact [6]

The two beams are supposed that have circular cross-section. The radii of beams are R_1 and R_2. The beam centerlines are represented two parameters $\boldsymbol{\xi}$ and $\boldsymbol{\eta}$ respectively. Therefore the centerlines of the beam are represented as $r_1(\xi)$ and $r_2(\eta)$. The curves $r_1(\xi)$ and $r_2(\eta)$ have the unique tangent vector at point $\boldsymbol{\xi}$ and $\boldsymbol{\eta}$, thus the curves are at least continuous in their partial derivative (C^1 continuity). As figure 3.1, the distance between beams is represented the function of $\boldsymbol{\xi}$ and $\boldsymbol{\eta}$ as

$$d(\xi,\eta) = \|r_1(\xi) - r_2(\eta)\| \ , \tag{3-1}$$

and when the distance is minimum, let the two parameters be ξ_c and η_c. In this closest point pair, the direction of distance vector and the beam centerline are perpendicular to each other. Therefore, the orthogonality conditions are satisfied as

$$p_1(\xi,\eta) = r_{1,\xi}^T\big(r_1(\xi) - r_2(\eta)\big) \quad \rightarrow \quad p_1(\xi_c,\eta_c) = 0 \ ,$$
$$p_2(\xi,\eta) = r_{2,\eta}^T\big(r_1(\xi) - r_2(\eta)\big) \quad \rightarrow \quad p_2(\xi_c,\eta_c) = 0 \ , \tag{3-2}$$

where $r_{i,\xi_j} = \frac{\partial r_i}{\partial \xi_j}$, is tangent vector of beam centerline.

And using distance, the gap function is created for detection of contact. The gap function is given as

$$g = d(\xi_c,\eta_c) - R_1 - R_2 \tag{3-3}$$

Using the gap function, contact is determined whether it occurs. If the gap function become a negative value, contact occurs between the beams. When contact occurs, the force and potential are applied between the beams. At this time, the closest centerline points (ξ_c,η_c) are used as the reaction force direction and size as follow,

$$\vec{f}_{c\varepsilon} = -\varepsilon\langle g\rangle\vec{n}, \tag{3-4}$$

where

$$\vec{n} = \frac{r_1(\xi_c) - r_2(\eta_c)}{\|r_1(\xi_c) - r_2(\eta_c)\|}, \qquad \langle g\rangle = \begin{cases} g, & g \le 0 \\ 0, & g > 0 \end{cases} .$$

In which, ε is the penalty parameter for the penalty method. The form of reaction force can be changed by the contact contribution method (penalty method or Lagrange multiplier or etc.). the process of contact determination and applying contact force is as shown figure 3.2.

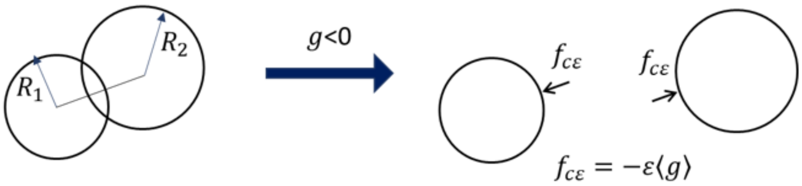

Figure 3.2 Diagram of contact situation

3.1.2 Penalty method

In equation (3-4), the penalty method is used for calculation of the contact force. In this condition, epsilon (ε) means the penalty parameter. As figure 3.3, the ideal condition is written $gf_{c\varepsilon} = 0$. However, the penetration between the beams is not allowed in the ideal condition. If use the ideal condition, solution can be unstable and oscillated. This unstable solution convergence is called 'chattering'. If use the penalty method, the penetration between the beams is allowed. The quantity of penetration is controlled by the penalty parameter ε, so proper penalty parameter should be determined according to problem cases. However, using the penalty method has better convergence than the ideal condition.

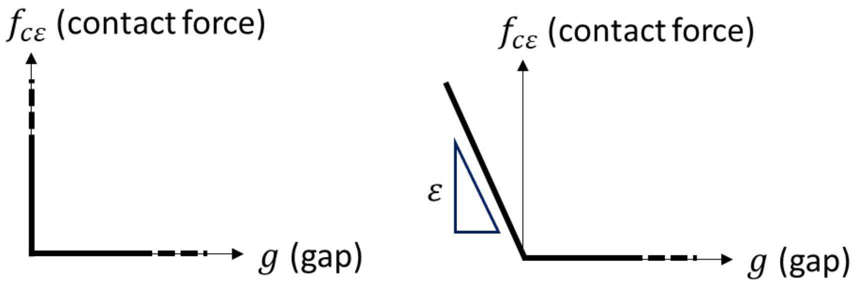

Figure 3.3 (left) Ideal contact force condition

(right) Contact force using penalty parameter

Lagrange multiplier method is also widely used like the penalty method. In the case of penalty method, the penalty parameter is constant value by problem cases. However, the Lagrange multiplier λ is determined by the solution process of the finite element analysis. If contact is occurred, the penalty method and the Lagrange multiplier method satisfy to the strain energy functions (potential equations) respectively as

$$\Pi = \Pi_{\mathrm{b1}} + \Pi_{\mathrm{b2}} + \Pi_{\mathrm{c}}, \tag{3-5}$$

where Π_{b1} and Π_{b2} are the potential from of two beams, and Π_{c} is the potential by contact condition as

$$\Pi_{\mathrm{c}} = \begin{cases} \dfrac{\varepsilon}{2} g^2 & \cdots \quad penalty \;\; method \\ \lambda g & \cdots \;\; Lagrange \;\; multiplier \end{cases}, \tag{3-6}$$

where g is gap function as equation (3-3). The form of gap function can be changed by the contact formulation method. The potential equation has solution in the extremal value of the equation, so the potential equation has the condition as

$$\delta\Pi = \delta\Pi_{\mathrm{b1}} + \delta\Pi_{\mathrm{b2}} + \delta\Pi_{\mathrm{c}} = 0 \;\; , \tag{3-7}$$

Using equation (3-7), the solutions of beam contact problem are obtained. As can be seen from the form of the contact potential, the Lagrange multiplier method behaves like the ideal condition as left of figure 3.3. The Lagrange multiplier method find the proper multiplier λ through potential equation, so the parameters do not need to be determined by problem cases. However, if use the Lagrange multiplier method, the solution convergence process can require additional equilibrium iterations because the solution convergence can be oscillated, in other words ‘chattering’. By comparison, the penalty method requires few equilibrium iterations compared to the Lagrange multiplier method. Besides, in case of multiple contact, the Lagrange multipliers are given at many points. This situation cause increasing in number of DOFs. In this thesis, the penalty method is used for good convergence and convenient formulation compared to the Lagrange multiplier method.

3.1.3 Formulation of point-to-point contact

The formulation of point-to-point contact refer to the reference [2], P. Wriggers, *On contact between three-dimensional beams undergoing large deflections.* Using the penalty parameter and the gap function, the potential by contact condition can be discretized. The potential term by contact condition is represented as

$$\Pi_{\mathrm{c}} = \frac{\varepsilon}{2} g^2 \ , \tag{3-8}$$

The finite element solution exist in an extremal value of Π, so δΠ becomes 0. Therefore, the variation of potential equation can write as

$$\delta\Pi = \delta\Pi_{\mathrm{b1}} + \delta\Pi_{\mathrm{b1}} + \delta\Pi_{\mathrm{c}} = \delta\Pi_{\mathrm{b1}} + \delta\Pi_{\mathrm{b1}} + \varepsilon g \cdot \delta g = 0 \ . \tag{3-9}$$

The linearization of equation (3-9) for the iteration of nonlinear equation is given as

$$\Delta\delta\Pi = \Delta\delta\Pi_{\mathrm{b1}} + \Delta\delta\Pi_{\mathrm{b1}} + \varepsilon\Delta g \cdot \delta g + \varepsilon g \cdot \varepsilon\Delta g \cdot \Delta\delta g \ . \tag{3-10}$$

Remind the orthogonality condition of two beam. Equation (3-2) is given as

$$\begin{cases} r_{1,\xi}^T\big(r_2(\eta) - r_1(\xi)\big) = \big(r_2(\eta) - r_1(\xi)\big) \cdot r_{1,\xi} = 0 \\ r_{2,\eta}^T\big(r_2(\eta) - r_1(\xi)\big) = \big(r_2(\eta) - r_1(\xi)\big) \cdot r_{2,\eta} = 0 \end{cases} , \tag{3-2a}$$

From this orthogonality condition, the linearization of the condition is obtained as

$$\begin{bmatrix} -r_{1,\xi} \cdot r_{1,\xi} + (r_2 - r_1) \cdot r_{1,\xi\xi} & r_{2,\eta} \cdot r_{1,\xi} \\ -r_{1,\xi} \cdot r_{2,\eta} & r_{2,\eta} \cdot r_{2,\eta} + (r_2 - r_1) \cdot r_{2,\eta\eta} \end{bmatrix} \begin{bmatrix} \Delta\xi \\ \Delta\eta \end{bmatrix} = \begin{bmatrix} -(r_2 - r_1) \cdot r_{1,\xi} \\ -(r_2 - r_1) \cdot r_{2,\eta} \end{bmatrix} \tag{3-11}$$

Using the linearization of the orthogonality condition, we get $\Delta g, \delta g, \Delta\delta g$. First, the gap function g is given by

$$g = \|r_2(\eta_c) - r_1(\xi_c)\| - (R_1 + R_2) \tag{3-3a}$$

The variation of the gap function is obtained using equation (3-3a) as

$$\delta g = [\delta r_2(\eta_c) - \delta r_1(\xi_c)] \cdot \vec{n}(\xi_c, \eta_c), \tag{3-12}$$

where $\vec{n}$ is the normal unit vector as follows,

$$\vec{n} = \frac{r_2(\eta_c) - r_1(\xi_c)}{\|r_2(\eta_c) - r_1(\xi_c)\|} \ . \tag{3-13}$$

Using $\delta x = x_{,\xi}\delta\xi + \delta u,$ equation (3-12) is rewritten as

$$\delta g = \big[\delta u_2(\eta_c) + r_{2,\eta}(\eta_c)\delta\eta_c - \delta u_1(\xi_c) - r_{1,\xi}(\xi_c)\delta\xi_c\big] \cdot \vec{n}(\xi_c, \eta_c), \tag{3-14}$$

according to the orthogonality condition, $r_{1,\xi}(\xi_c) \cdot \vec{n}(\xi_c, \eta_c) = r_{2,\eta}(\eta_c) \cdot \vec{n}(\xi_c, \eta_c) = 0$, so equation (3-14) is rewritten as

$$\delta g = [\delta u_2(\eta_c) - \delta u_1(\xi_c)] \cdot \vec{n}(\xi_c, \eta_c), \tag{3-15}$$

The linearization of the gap function goes through same process to variation, so the linearization of the gap function is represented as

$$\Delta g = [\Delta u_2(\eta_c) - \Delta u_1(\xi_c)] \cdot \vec{n}(\xi_c, \eta_c). \tag{3-16}$$

From equation (3-12), the linearization of the variation of the gap function is obtained as

$$\Delta\delta g = [\Delta\delta r_2(\eta_c) - \Delta\delta r_1(\xi_c)] \cdot \vec{n}(\xi_c, \eta_c) + [\delta r_2(\eta_c) - \delta r_1(\xi_c)] \cdot \Delta\vec{n}(\xi_c, \eta_c), \tag{3-17}$$

where $\Delta\vec{n}$ is given from equation (3-13) as

$$\Delta\vec{n} = \frac{1}{\|r_2(\eta_c) - r_1(\xi_c)\|}(1 - \vec{n} \otimes \vec{n})\big(\Delta r_2(\eta_c) - \Delta r_1(\xi_c)\big), \tag{3-18}$$

and using $\delta x = x_{,\xi}\delta\xi + \delta u$, equation (3-18) is rewritten as

$$\Delta\vec{n} = \frac{1}{\|r_2(\eta_c) - r_1(\xi_c)\|}(1 - \vec{n} \otimes \vec{n})\big(\Delta u_2 + \Delta r_{2,\eta}\Delta\eta - \Delta u_1 - \Delta r_{1,\xi}\Delta\xi\big), \tag{3-19}$$

Using equation (3-19) and $\delta x = x_{,\xi}\delta\xi + \delta u$ and the linearization of the orthogonality condition at ξ_c, η_c, equation (3-17) is rewritten as

$$\Delta\delta g = \left[(\delta u_2)_{,\eta}\Delta\eta_c - (\delta u_1)_{,\xi}\Delta\xi_c\right]\cdot\vec{n} + \left[(\Delta u_2)_{,\eta}\delta\eta_c - (\Delta u_1)_{,\xi}\delta\xi_c\right]\cdot\vec{n} + \left[r_{2,\eta\eta}\delta\eta_c\Delta\eta_c - r_{1,\xi\xi}\delta\xi_c\Delta\xi_c\right]\cdot\vec{n}$$
$$+\frac{1}{\|r_2(\eta_c) - r_1(\xi_c)\|}\left[\delta u_2 + r_{2,\eta}\delta\eta - \delta u_1 - r_{1,\xi}\delta\xi\right]\cdot(1 - \vec{n}\otimes\vec{n})\big(\Delta u_2 + r_{2,\eta}\Delta\eta - \Delta u_1 - r_{1,\xi}\Delta\xi\big) \tag{3-20}$$

In equation (3-20), $\Delta\xi_c, \Delta\eta_c$ is solved the linearized orthogonality condition equation (3-11) at closest points ξ_c, η_c as follow

$$[\mathrm{A}]\begin{bmatrix}\Delta\xi_c\\ \Delta\eta_c\end{bmatrix} = [B]\begin{bmatrix}\Delta u_1\\ \Delta u_2\end{bmatrix} + [\mathrm{C}]\begin{bmatrix}\Delta u_{1,\xi}\\ \Delta u_{2,\eta}\end{bmatrix}, \tag{3-21}$$

where the matrices A,B and C is given by

$$[\mathrm{A}] = \begin{bmatrix}-r_{1,\xi}\cdot r_{1,\xi} + (r_2 - r_1)\cdot r_{1,\xi\xi} & r_{2,\eta}\cdot r_{1,\xi}\\ -r_{1,\xi}\cdot r_{2,\eta} & r_{2,\eta}\cdot r_{2,\eta} + (r_2 - r_1)\cdot r_{2,\eta\eta}\end{bmatrix},$$
$$[\mathrm{B}] = \begin{bmatrix}r_{1,\xi}^T & -r_{1,\xi}^T\\ r_{2,\eta}^T & -r_{2,\eta}^T\end{bmatrix}, \qquad [\mathrm{C}] = \begin{bmatrix}-(r_2 - r_1)^T & 0^T\\ 0^T & -(r_2 - r_1)^T\end{bmatrix}. \tag{3-22}$$

In equation (3-22), all quantities are obtained with respect to the closest points ξ_c, η_c.

For obtain the finite element solution, the linearization of displacement is needed [4]. The displacement with respect to the centerline of beam is given by

$$\vec{u_i} = H_i(\xi_i)\vec{u}_{ik},$$

So, equation (3-21) can be expressed as

$$\begin{bmatrix}\Delta\xi_c\\ \Delta\eta_c\end{bmatrix} = [A]^{-1}\left\{[B]\begin{bmatrix}H_1 & 0\\ 0 & H_2\end{bmatrix} + [\mathrm{C}]\begin{bmatrix}H_{1,\xi} & 0\\ 0 & H_{2,\eta}\end{bmatrix}\right\}\begin{bmatrix}\Delta u_{1k}\\ \Delta u_{2k}\end{bmatrix} = [\mathrm{D}]\begin{bmatrix}\Delta u_{1k}\\ \Delta u_{2k}\end{bmatrix}, \tag{3-23}$$

In similar to equation (3-23), the variation of ξ_c, η_c is also obtained as

$$\begin{bmatrix}\delta\xi_c\\ \delta\eta_c\end{bmatrix} = [\mathrm{D}]\begin{bmatrix}\delta u_{1k}\\ \delta u_{2k}\end{bmatrix}, \tag{3-24}$$

So, the contact contribution by the penalty method is expressed as

$$\Delta\delta\Pi_{\mathrm{c}} = (\delta u_{1k}^T, \delta u_{2k}^T)[K_c](\Delta u_{1k}, \Delta u_{2k})^T, \tag{3-25}$$

$$\delta\Pi_{\mathrm{c}} = (\delta u_{1k}^T, \delta u_{2k}^T)[R_c], \tag{3-26}$$

where

$$K_{\mathrm{c}} = \varepsilon\cdot\left\{\begin{bmatrix}-H_{1,\xi}^T\\ H_{2,\eta}^T\end{bmatrix}\vec{n}\cdot\vec{n}^T[-H_{1,\xi} \quad H_{2,\eta}]\right\} + \varepsilon\cdot g\left\{\begin{bmatrix}-H_1^T\vec{n} & 0\\ 0 & H_2^T\vec{n}\end{bmatrix}[D]\right.$$
$$\left. +[D]^T\begin{bmatrix}-\vec{n}^T H_1 & 0\\ 0 & \vec{n}^T H_2\end{bmatrix} + [D]^T\begin{bmatrix}-\vec{n}^T r_{1,\xi\xi} & 0\\ 0 & \vec{n}^T r_{2,\eta\eta}\end{bmatrix}[D]\right.$$

$$+\frac{1}{g}\cdot\left\{\left[-H_{1,\xi}\ \ H_{2,\eta}\right]+\left[-r_{1,\xi}\ \ r_{2,\eta}\right][D]\right\}^{T}(1-\vec{n}\cdot\vec{n}^{T})\cdot\left\{\left[-H_{1,\xi}\ \ H_{2,\eta}\right]+\left[-r_{1,\xi}\ \ r_{2,\eta}\right][D]\right\}\Bigg), \tag{3-27}$$

and

$$R_c = \ \ \varepsilon g\begin{bmatrix}-H_{1,\xi}^{T}\vec{n}\\ H_{2,\eta}^{T}\vec{n}\end{bmatrix}. \tag{3-28}$$

3.2 Improved formulation – non-circular cross-sections

3.2.1 Beam-to-beam contact between rectangular cross-section beams

P. Litewka and P. Wriggers suggested contact between 3D beams with rectangular cross-sections at 2002 [4]. The beam elements are used 3D rectangular Timoshenko beam formulation.

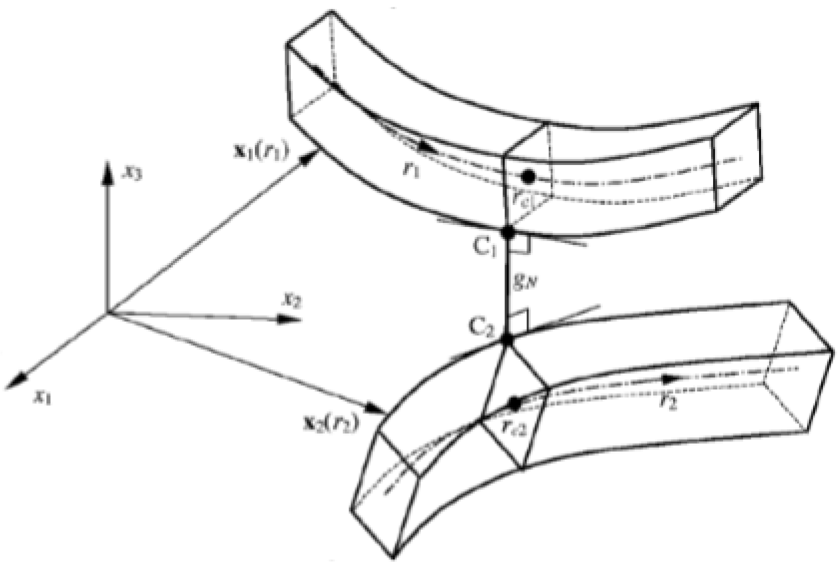

Figure 3.4 A pair of contacting beams with rectangular cross-sections [4]

Existing point-to-point contact formulation is formulated based on the beam centerlines. However, this contact formulation is developed on the edges of beam. The positions and displacements of the beam edges are obtained through the positions and displacements of the beam centerline and the rotation of nodal points at beam elements. So, using the positions of edges, minimal distances and closest points between edges of beams are obtained through the distance searching processes. Because one beam element has four edges, the contact possibility should be determined at which corners will contact. This paper suggest that two closest edges on beam per another beam centerline are checked.

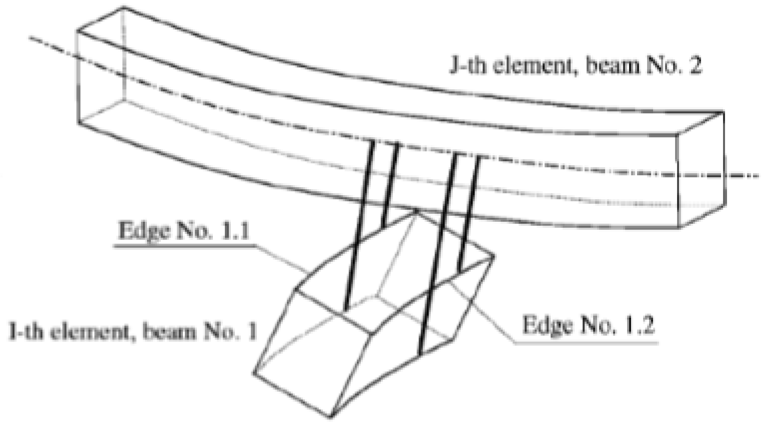

Figure 3.5 Contact search – two closest edges per beam centerline [4]

For example, as figure 3.5, two edges 1.1 and 1.2 from the beam no.1 are closest with the beam no.2. Similar to, two edges 2.1 and 2.2 from the beam no.2 are closest with the beam no.1. Therefore, four edge pairs as 1.1 and 2.1, 1.1 and 2.2, 1.2 and 2.1, 1.2 and 2.2, are checked whether contact is occurred or not.

This formulation change cross-section from circular cross-section to rectangular cross-section. However the beam contact formulation still cannot solve for arbitrary cross-section as I-beam, H-beam, quadrilateral cross-section or curved cross-section. Further, if ratio width and height of rectangular cross-section is big difference, searching process can undergo error.

3.2.2 Beam-to-beam contact between curbed cross-section beams

A. G. Neto suggested contact between 3D beams with curve shape cross-sections at 2016 [8]. The surfaces of the beam are given by the convective coordinate systems.

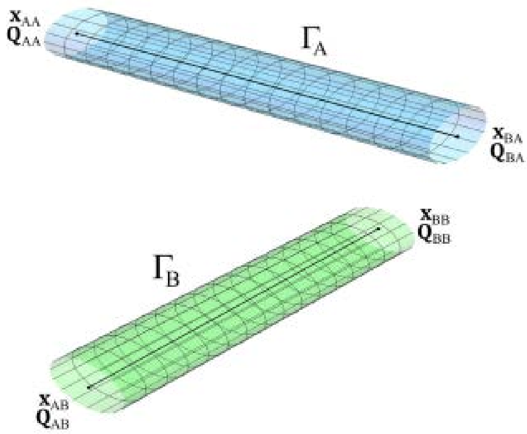

Figure 3.6 Beam-to-beam contact with curved surfaces [8]

Surfaces depended the convective coordinate are represented as

$$\Gamma_A = \Gamma_A(\zeta_A, \theta_A, \vec{d}_A), \Gamma_A = \Gamma_B(\zeta_B, \theta_B, \vec{d}_B), \tag{3-29}$$

where ζ_i, θ_i are the convective coordinates and $\vec{d}_i$ is the generalized displacements vector.

From these surface functions, the orthogonality conditions are given by

$$\begin{cases} \Gamma_{\mathrm{A},\zeta_A} \cdot (\Gamma_\mathrm{A} - \Gamma_\mathrm{B}) = 0 \\ \Gamma_{\mathrm{A},\theta_A} \cdot (\Gamma_\mathrm{A} - \Gamma_\mathrm{B}) = 0 \\ \Gamma_{\mathrm{B},\zeta_B} \cdot (\Gamma_\mathrm{A} - \Gamma_\mathrm{B}) = 0 \\ \Gamma_{\mathrm{B},\theta_B} \cdot (\Gamma_\mathrm{A} - \Gamma_\mathrm{B}) = 0 \end{cases} \tag{3-30}$$

Because of these conditions, surfaces respected to the convective variables are required at least continuous in their partial derivative, thus C^1-continuous. Using these surface representations, the surface parameterization and the cross-sections of beams are given as

$$\Gamma(\zeta,\theta) = \vec{x}(\zeta) + \vec{a}(\zeta,\theta) \tag{3-31}$$

where $\vec{x}(\zeta)$ is the description of beam axis, and $\vec{a}(\zeta,\theta)$ is the positions of material positions at the beam surface. $\vec{a}(\zeta,\theta)$ has the cross-section information and cross-section orientation by rotation.

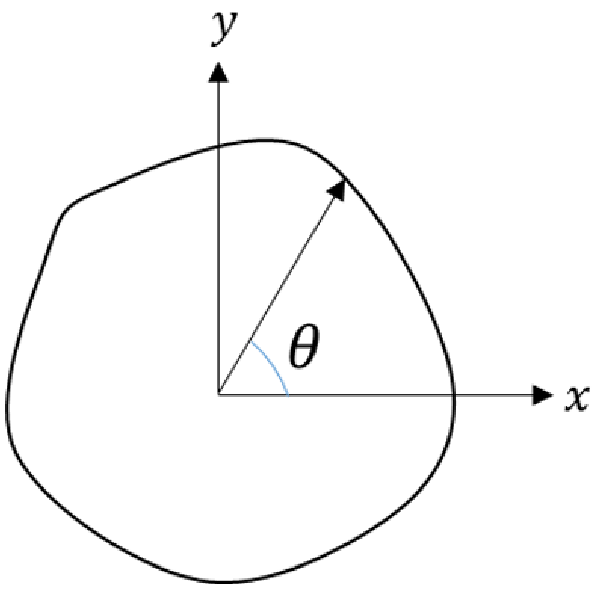

Figure 3.7 Cross-section and convective coordinate

The contact points are given as one closest point pair, differently to case of rectangular cross-section. Using convective coordinates, cross-section can be made close to the rectangular shape for the superellipse curve. However, if surface is not satisfied at least C^1-continuous or surface has a severe inflection, the contact process can fail for the contact formulation, so, in order to describe the arbitrary cross-section, the convective coordinate is not enough, and other beam elements and formulation are needed.

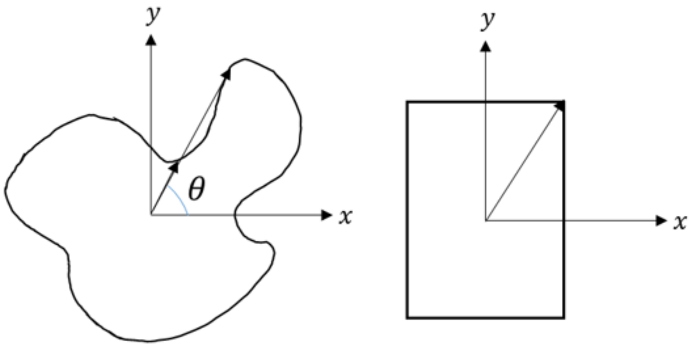

Figure 3.8 Severe inflection, sharped shape (not satisfied $\boldsymbol{C^1}$-continuous)

3.2 Improved formulation – multiple contact formulation

3.2.1 Concept of line-to-line contact

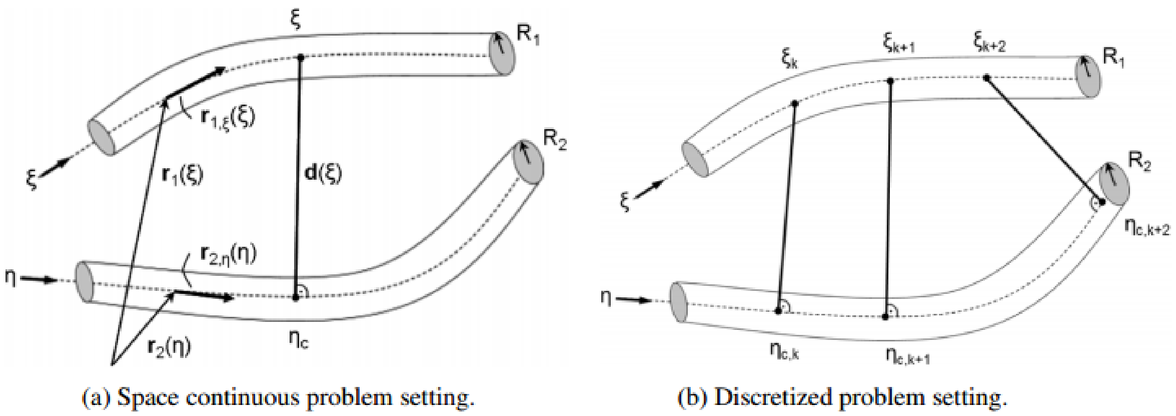

Figure 3.9 Kinematics of line-to-line contact [6]

In line-to-line contact, the minimum distance is not fixed value. From point $r_1(\xi)$ on the slave element, the closest points $r_2(\eta_c)$ are found. Finally, the minimum distances become function of point on the slave element. If the points on the slave elements are discretized, the slave points have the closest points on the master element. The closest point η_c in the master beam to a given slave point ξ is determined by the minimal distance function as follow,

$$d_{ul}(\xi) = \min d(\xi,\eta) = d(\xi,\eta_c) \ , \tag{3-32}$$

in which, the distance function is given by $d(\xi,\eta) = \|r_1(\xi) - r_2(\eta)\|$.

In similar to the point-to-point contact, the orthogonality condition is given, but compared to the point-to-point contact, only one condition is given as

$$p_2(\xi,\eta) = r_{2,\eta}^T\big(r_1(\xi) - r_2(\eta)\big) \quad \rightarrow \quad p_2(\xi,\eta_c) = 0 \ , \tag{3-33}$$

As you can see from the equation (3-33), the orthogonality condition consists of a function for slave point ξ, so the closest master point η_c is determined according to the slave point ξ.

Using the minimal distance function, equation (3-32), the gap function is suggested for contact determination.

The gap function also represented the function by points on slave elements as

$$g(\xi) = d_{ul}(\xi) - R_1 - R_2 \tag{3-34}$$

From the gap function, contact determined whether it occurs. Similar to the point-to-point contact, if the gap function become negative value, contact occurs between the beams, but the gap function form the field along the slave beam in line-to-line contact case. Because the gap function is changed from the determined constant to the function of slave point, the potential of contact by the penalty method is changed as

$$\Pi_c = \frac{1}{2}\ \varepsilon \int_0^{l_1} \langle g(\xi)\rangle^2\, ds_1, \tag{3-35}$$

where l_1 is length of the slave beam, and the gap function according to contact condition is given by

$$\langle g(\xi)\rangle = \begin{cases} g(\xi), & g(\xi) \le 0 \\ 0, & g(\xi) > 0 \end{cases},$$

and the contact force vector and the normal vector are given by

$$\vec{f}_{c\varepsilon} = -\varepsilon\langle g(\xi)\rangle \vec{n}(\xi),$$

$$\vec{n}(\xi) = \frac{r_1(\xi) - r_2(\eta_c)}{\|r_1(\xi) - r_2(\eta_c)\|},$$

As you can see the form of contact force and normal vector, these are parametrized to the slave point ξ.

The process of contact determination and applying the contact force is as shown figure 3.2. Because the gap function is parametrized, the reaction force also becomes a function. The reaction force is applied as a distributed load.

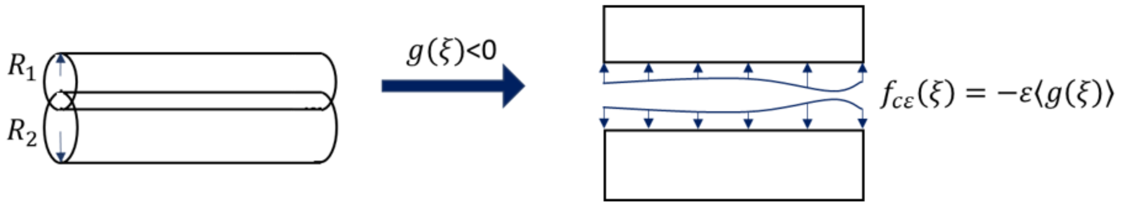

Figure 3.10 diagram of line-to-line contact situation

In the point-to-point contact formulation, the unique closest point pair is required for developing the contact formulation. However, two beams can contact at multiple points depending on the geometrical configuration of beams, for example, two parallel beams or between straight beam and helical beam. Depending on the angle between the two beam elements, the unique closest point condition can be broken and has error by geometrical configuration. C. Meier suggested the contact angle condition to can use the point-to-point contact. [6]

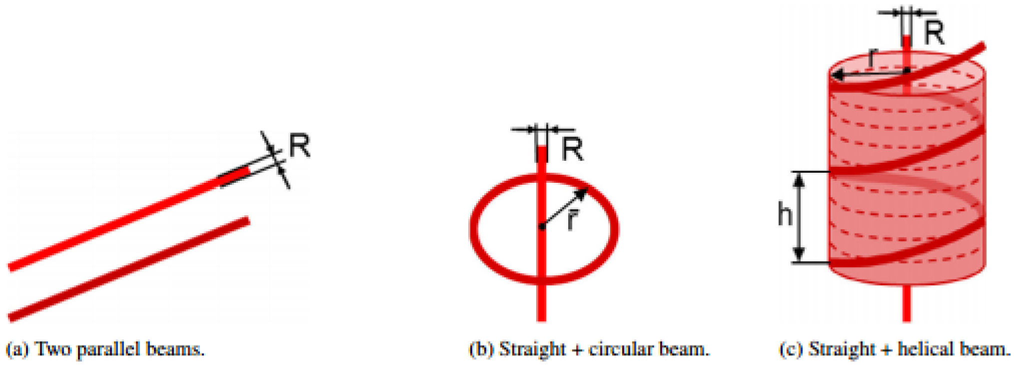

Figure 3.11 Different geometrical configurations concerning contact angle and curvature [6]

The maximal cross-section to curvature radius ratio is given by

$$\mu_{max} = \frac{R}{min(\frac{1}{\bar{\kappa}})} \quad , \tag{3-36}$$

where $\bar{\kappa} = \|r_{,ss}\|$, with $s \in [0; \tilde{l}]$ is the coordinate according to the arc-length of the current, and the lower bound for the contact angle is given by

$$\alpha > \alpha_{min} = \arccos(1 - 2\mu_{max}) \tag{3-37}$$

Figure 3.12 Contact of two beams given contact angle **α** [7]

You can refer to the reference paper [8] for detailed derived process. The line-to-line formulation search all discretized point in the slave beam, so the calculation accuracy is higher, but the time performance is poor than the point-to-point contact method. Therefore, the line-to-line method and point-to-point method should be selected depending on the problem situation. Similar to the point-to-point contact, the line-to-line contact formulation is also developed based circular cross-section. If use the line-to-line contact formulation at arbitrary cross-section, the maximal cross-section to curvature radius ratio should be redefined according to the shape of the cross-section.

Chapter 4. Contact Algorithm

In this chapter, the contact detection algorithm is introduced. The process of closest point searching and determination of contact are explained.

Before applying force, the closest surface points are searched through global and local search. In the local search, the contact possibility of the element edges are determined because of decreasing in cost. After the closest edge points are searched, the external forces are applied. If the beam converge through force step without contact force, the contact determination is performed. If contact occurs between the beams, the contact forces are applied until the gap is converged in the tolerance.

4.1. Global and local search

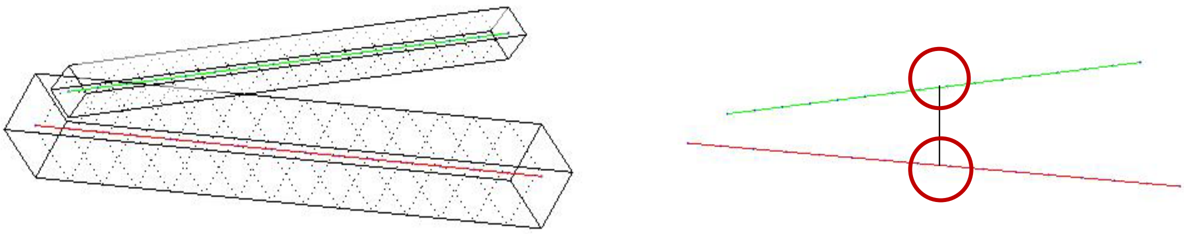

Figure 4.1 Global search – searching between beam nodes

Using the beam nodes, the closest nodal points are searched. If a beam is circular cross-section, the direction between the closest nodal points on the beam centerline and the direction between the closest surface points on the beam are same direction, and the closest surface points are on the line connecting the closest nodal points, so the contact forces apply on a same position in the two cases. However, in case of an arbitrary cross-section, the closest surface points may not be on the line connecting the closest nodal points, so applied points of the contact force are different in the two cases. Therefore, the closest surface or edge points should be searched. However, searching along all discretized surface or edge points takes a lot of time, so the closest surface points are searched based on the found closest nodal points. This process of finding the closest nodal point is called ‘global search’.

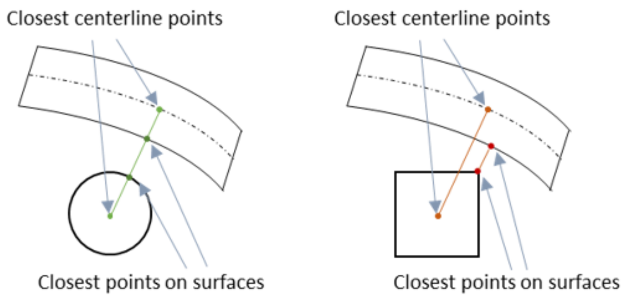

Figure 4.2 Difference of closest points with circular and arbitrary cross-section

Based on the found closest nodal points, the closest surface point searching is performed between edges of the cross-sectional plane about the beam centerline point. Let call it 'local search'. The local search is performed together with both side elements of the element with the closest nodal points. For example, if closest nodal points are in the element *i* in one beam and in the element *j* in another beam respectively, elements from *i*-1 to *i*+1 in one beam and elements from *j*-1 to *j*+1 are used in searching of the closest surface points. In the candidate elements using searching, the beam centerline discretize through the interpolation of beam nodal points on the element. This centerline points have each cross-section including the centerline point. For searching of the closest surface points, the edges of cross-section including each centerline point are used.

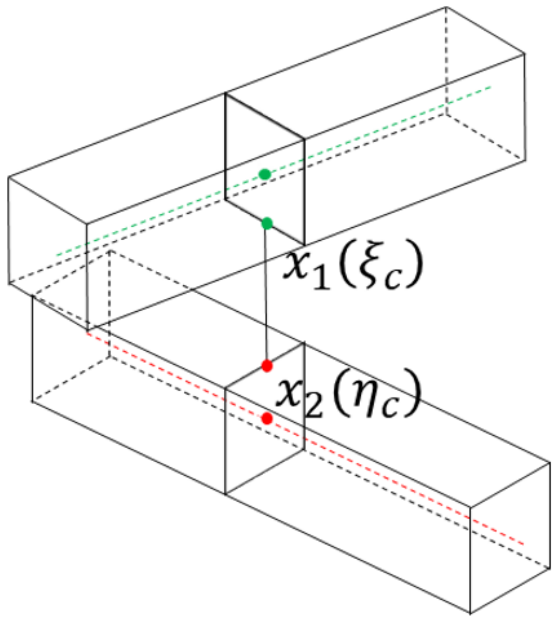

Figure 4.3 Local search – searching between beam edges

The local search is performed between edges of cross-section including the discretized beam centerline point. If searching is performed for all edges, it takes a lot of time. Therefore, the contact possibility of edge is determined using the positional relationships between the cross-sections. At the first time, the edges are determined whether the edges are in the surface or not. The edges in inner side are not used for the local search. This possibility information is given by the cross-sectional shape and placement of the cross-sectional elements, so the possibility information does not change by the geometry configuration of beams, thus it can be given as initial information.

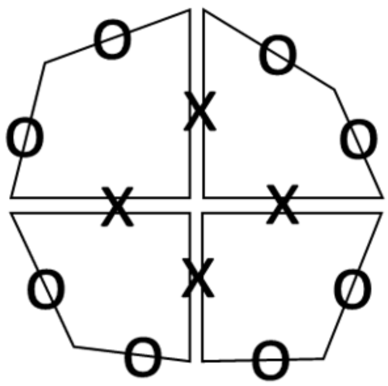

Figure 4.4 Contact possibility determination – First step

To the next, the positional relationships between elements of the cross-section are used in determination of contact possibility. If dot product between the relative position vector and the normal vector of edge is positive, then that edge can contact and the edge is used for local search. This contact possibility information is changed by the geometrical configuration of beams, so the possibility is checked in each step between each cross-sectional elements.

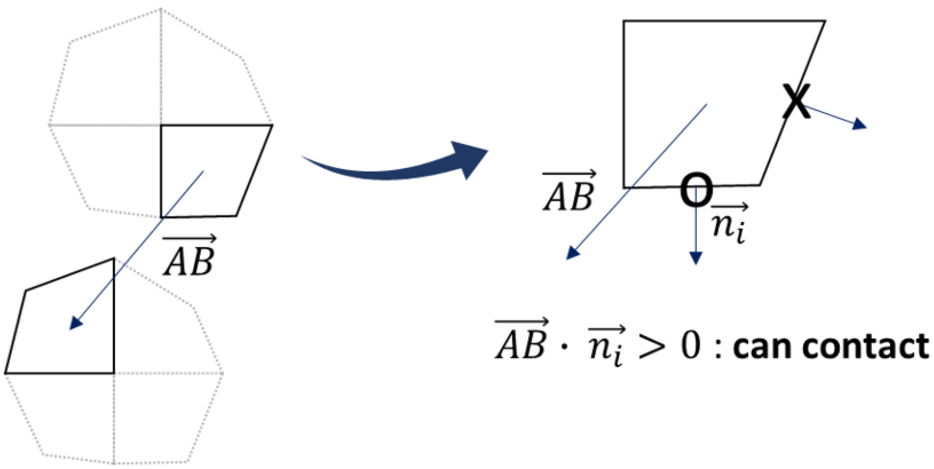

Figure 4.5 Contact possibility determination – Second step

Using the contact possibility information by two determination steps, the closest surface points on beams are searched faster than case without possibility information. Through the local search, information as beam centerline points on the cross-section of the closest surface point, edge with the closest surface points and the positions of the closest surface points are saved. If there are a multiple cross-sectional elements, this information is recorded every number of cases that can contact between the cross-sectional elements.

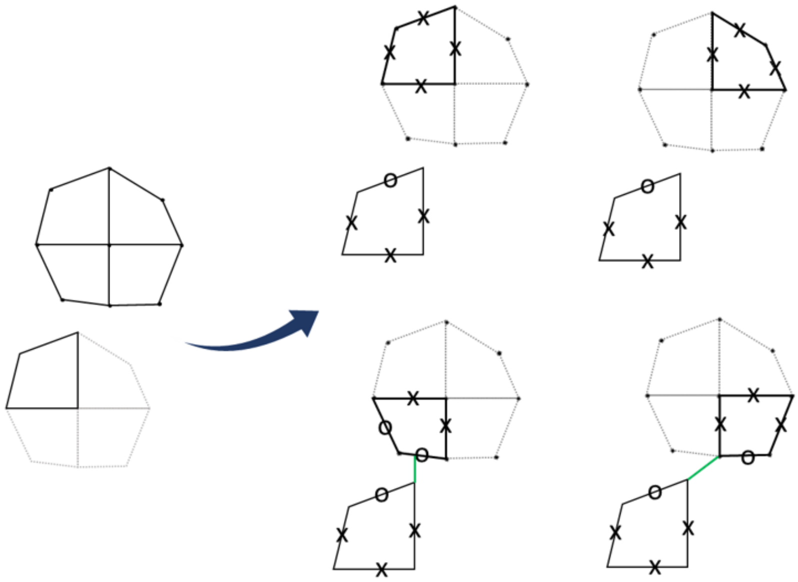

Figure 4.6 Closest points are checked between every cross-sectional elements

4.2. Contact determination

Let discuss new contact determination method by comparing with the existing contact search method

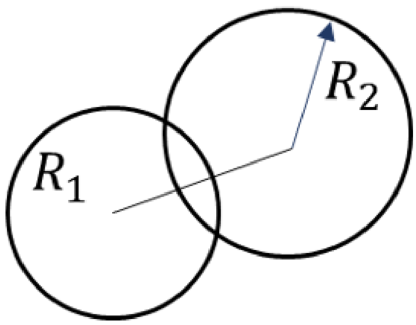

Figure 4.7 Contact search of circular cross-section

In case of a circular cross-section, contact is determined using the radii of beams. The contact condition is giving as $g = d - R_1 - R_2 < 0$. This contact search method is very simple, but it cannot use in noncircular cross section. Searching of the closest points is performed along the beam centerline. Therefore, this method applies the contact force toward the center of beams. As figure 4.2, the position and direction applied the contact force are different between case of applied in the center of beam and case of applied in the edge or surface of beams. Many noncircular cross section cases is applied the contact force in various direction.

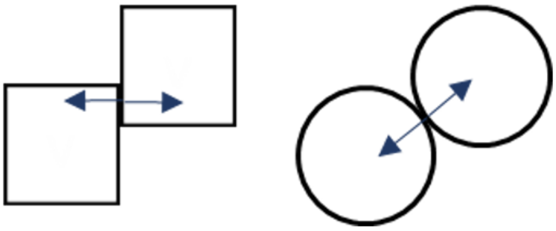

Figure 4.8 Difference of applying contact force on circular and non-circular cross-sections

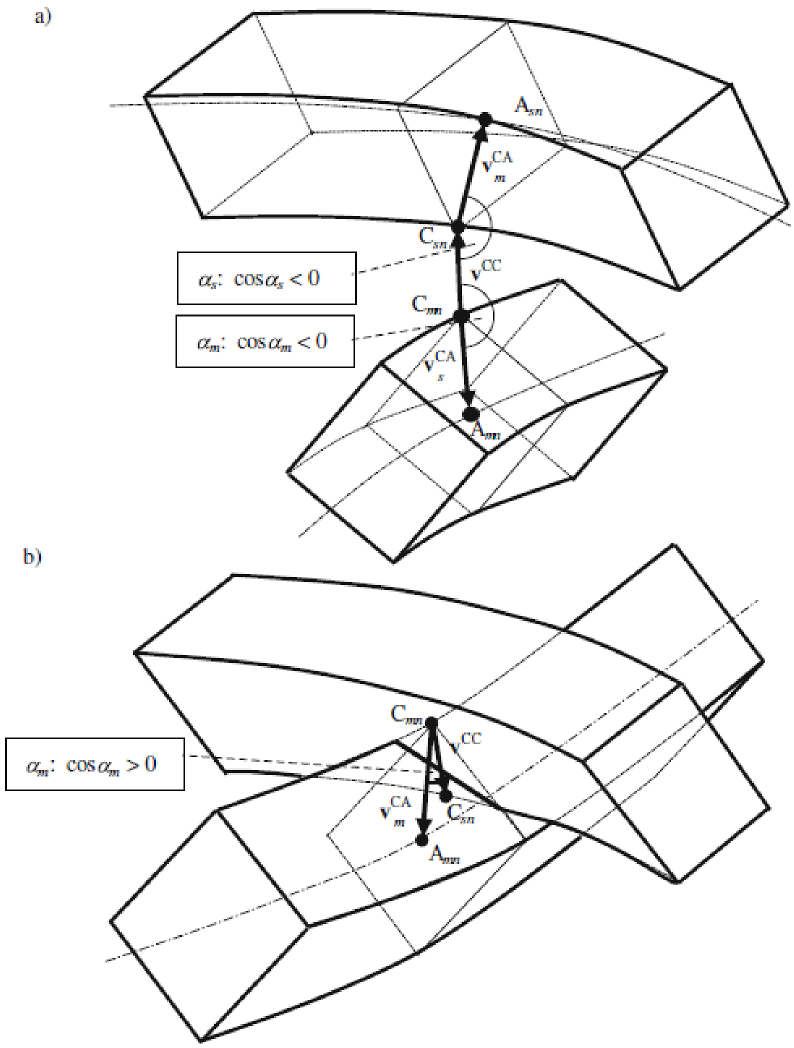

Figure 4.9 Contact search of rectangular cross-section [4]

P. Litewka, P. Wriggers, suggests the contact determination method in 2002 [4]. In case of rectangular cross-section, contact is determined in the edge points of beams. As figure 4.7, the closest edge points are C_{sn} and C_{mn} respectively, and the beam centerline points of the cross-section where the closest edge points exist are A_{sn} and C_{mn} respectively. The distance vector connecting edge points C_{sn}, C_{mn} and the vector connecting points edge point and beam centerline point make angles. This angle is α_s and α_m respectively. Using this two angle, the contact condition is giving as $\cos\alpha_m < 0, \cos\alpha_s < 0$.

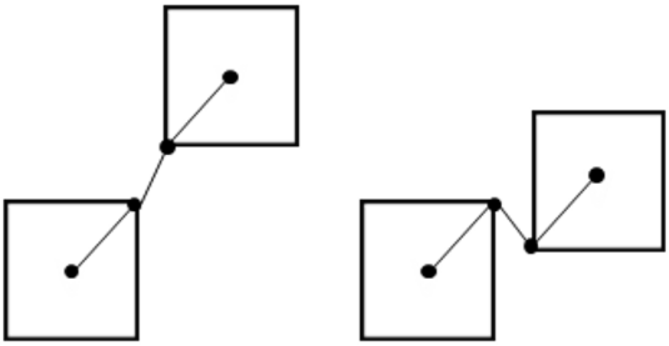

Figure 4.10 Unstable example of edge contact searching

This method cannot use in non-rectangular cross section even case of quadrilateral cross section, and there are counter examples in extreme cases and often unstable searching results are shown in some cases, especially two beams or two cross-sections are parallel, problem can occur as figure 4.10.

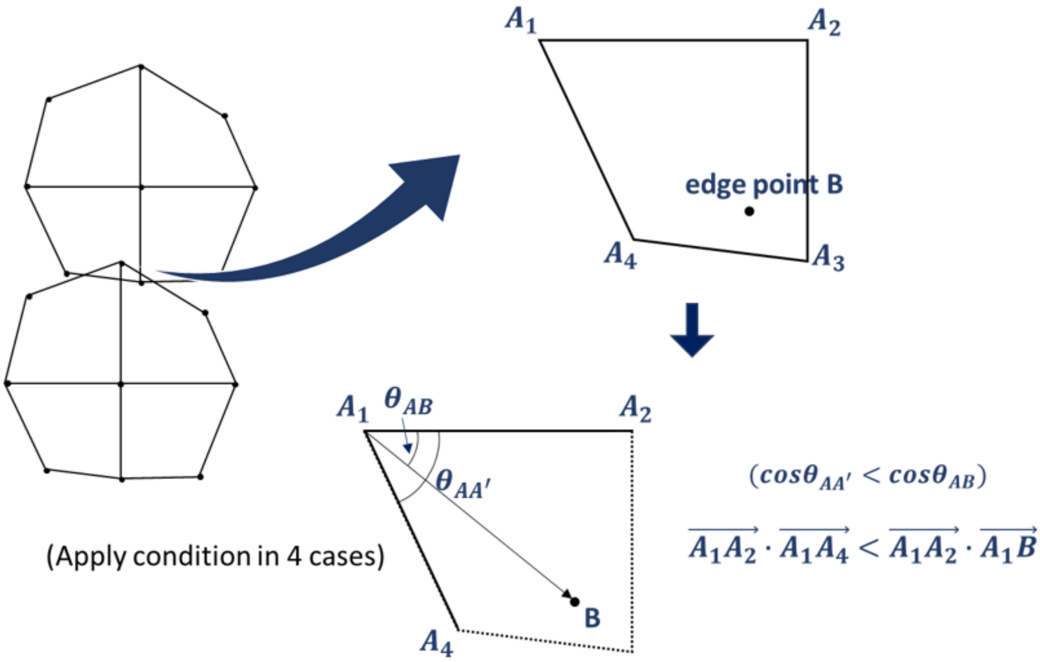

Figure 4.11 Contact search of arbitrary cross-section

New contact determination method is used arbitrary cross-sections. The plane elements are divided into several quadrilateral elements. Figure 4.11 is the cross-section that has the closest points searched by global and local searching, and the edge point B found in local search is used contact determination process. About the edge point B on the beam B, the point B can lie on other plane element on the cross-section having the closest points on beam A. To determine whether the point B is in the plane element on the beam A, the contact determination process is performed as

$$\begin{aligned}
&\overrightarrow{A_1A_2} \cdot \overrightarrow{A_1A_4} < \overrightarrow{A_1A_2} \cdot \overrightarrow{A_1B} \\
&\overrightarrow{A_2A_3} \cdot \overrightarrow{A_2A_1} < \overrightarrow{A_2A_3} \cdot \overrightarrow{A_2B} \\
&\overrightarrow{A_3A_4} \cdot \overrightarrow{A_3A_2} < \overrightarrow{A_3A_4} \cdot \overrightarrow{A_3B} \\
&\overrightarrow{A_4A_1} \cdot \overrightarrow{A_4A_3} < \overrightarrow{A_4A_1} \cdot \overrightarrow{A_4B}
\end{aligned} \tag{4-1}$$

where point A_1, A_2, A_3, A_4 is the cross-sectional nodal point of plane element on beam A, and point B is the edge point B found in the closest point searching. The detailed situation is shown in the figure 4.11. If four conditions of equation (4-1) are satisfied all, searching method determine that contact occur. Because the contact determination method use the geometrical configuration of the cross-sectional plane element, this method can be performed not only rectangular elements but also any quadrilateral elements. For using this method, the edges of plane element should be straight line. If the edges are not straight line as curve, the shape needs to be replaced by several straight lines. In addition, internal angle of quadrilateral element is not more than 180 degrees. If plane elements are not quadrilateral but polygon shape with more than four edges, condition equations (4-1) increase to the number of edges. For example, the plane element is octagonal shape, condition equations increase to 8 equations. However, plane element has severe inflection as I-shape or H-shape or etc., the plane element should be divided to sub-elements as convex shape or quadrilateral shape that internal angle is not more than 180 degrees.

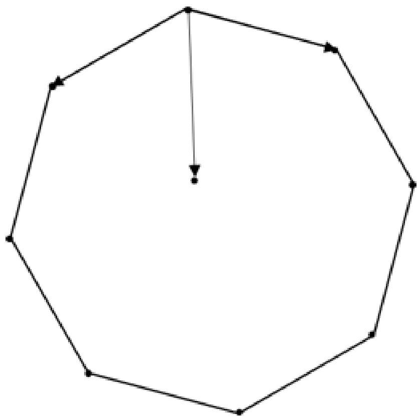

Figure 4.12 Octagonal shape example – this case requires eight condition equations

4.3. Contact formulation

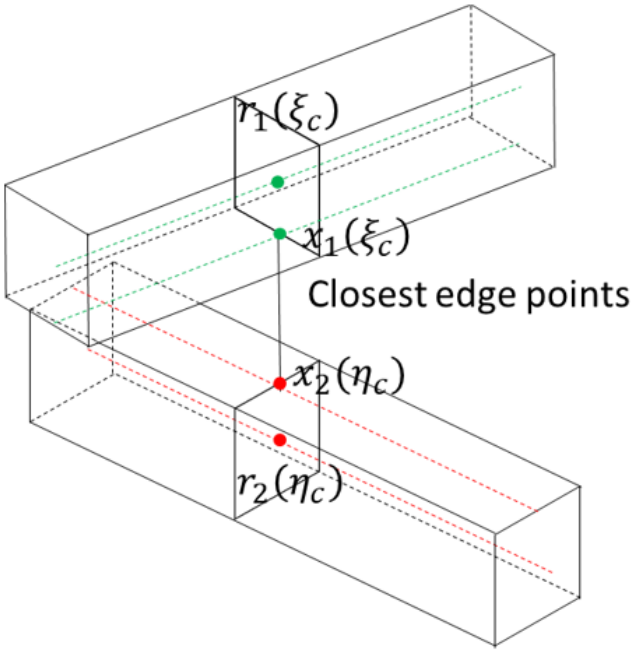

Figure 4.13 A pair of beams and closest edge points

The contact formulation process is similar to formulation of the point-to-point contact. However, the point-to-point contact is developed the formulation about the beam centerline. Therefore, the formulation process is modified from about the beam centerline to about the line of beam surface, and the line of beam surface is represented a parameter of the beam node. The formulation of point-to-point contact is in chapter 3.1.1 and 3.1.3. Here is review of point-to-point contact as

- Orthogonality condition

$$\begin{cases} r_{1,\xi}^T\left(r_2(\eta)-r_1(\xi)\right)=\left(r_2(\eta)-r_1(\xi)\right)\cdot r_{1,\xi}=0 \\ r_{2,\eta}^T\left(r_2(\eta)-r_1(\xi)\right)=\left(r_2(\eta)-r_1(\xi)\right)\cdot r_{2,\eta}=0 \end{cases}, \tag{3-2a}$$

- Gap function

$$g=\|r_2(\eta_c)-r_1(\xi_c)\|-(R_1+R_2) \tag{3-3a}$$

- Normal unit vector

$$\vec{n}=\frac{r_2(\eta_c)-r_1(\xi_c)}{\|r_2(\eta_c)-r_1(\xi_c)\|}\ . \tag{3-13}$$

As you can see from the equations, the point-to-point contact formulation is developed along the beam centerlines, $r_1(\xi)$ and $r_2(\eta)$. The position vector of 3D degenerated beam in chapter 2 is given by

$$\vec{x}^{(m)}=\sum_{k=1}^{q}h_k(r)\overrightarrow{x_k}+\sum_{k=1}^{q}h_k(r)\,\bar{y}_k{}^{(m)}\overrightarrow{V_{\bar{y}}}^k+\sum_{k=1}^{q}h_k(r)\,\bar{z}_k{}^{(m)}\overrightarrow{V_{\bar{z}}}^k, \tag{2-4}$$

where

$$\bar{y}_k{}^{(m)} = \sum_{k=1}^{p} h_j(s,t)\bar{y}_k{}^{j(m)}, \qquad \bar{z}_k{}^{(m)} = \sum_{k=1}^{p} h_j(s,t)\bar{z}_k{}^{j(m)}, \tag{2-5}$$

In equation (2-4) and (2-5), the coordinate r is longitudinal direction and s, t are tangential direction on the cross-section. In closest surface points, the tangential line at the closest point on beam surface consist of the parameter r, and the cross-sectional parameters s, t are fixed value by position of the closest point. So tangential line at the closest point $x_1(\xi_c)$ is given by

$$\overrightarrow{x_1} = \overrightarrow{x_1}(r, s_c, t_c) = \overrightarrow{x_1}(\xi, s_c, t_c) = \overrightarrow{x_1}(\xi) \tag{4-2}$$

where s_c, t_c are the fixed value by determining of the closest point. To configure the tangential line $\overrightarrow{x_2}$ on another beam, same process applies to another beam. Using the surface tangential line $\overrightarrow{x_1}$ and $\overrightarrow{x_2}$, the formulations of point-to-point contact are modified as

- Orthogonality condition

$$\begin{cases} \vec{x}_{1,\xi}^T\left(\vec{x}_2(\eta) - \vec{x}_1(\xi)\right) = \left(\vec{x}_2(\eta) - \vec{x}_1(\xi)\right) \cdot \vec{x}_{1,\xi} = 0 \\ \vec{x}_{2,\eta}^T\left(\vec{x}_2(\eta) - \vec{x}_1(\xi)\right) = \left(\vec{x}_2(\eta) - \vec{x}_1(\xi)\right) \cdot \vec{x}_{2,\eta} = 0 \end{cases}, \tag{4-3}$$

- Gap function

$$g = \|\vec{x}_2(\eta_c) - \vec{x}_1(\xi_c)\| \tag{4-4}$$

- Normal unit vector

$$\vec{n} = \frac{\vec{x}_2(\eta_c) - \vec{x}_1(\xi_c)}{\|\vec{x}_2(\eta_c) - \vec{x}_1(\xi_c)\|} \ . \tag{4-5}$$

These conditions (4-3) to (4-5) are applied the process of contact formulation in chapter 3.1.3.

Chapter 5. Numerical Results

5.1 Confirmation of difference between 3D beam and 3D solid element

For validation of the contact formulation, commercial software ANSYS is used in the validation examples. However, only contact between circular beams is possible in ANSYS. Most of commercial software are not supported beam contact between non-circular beams. Therefore, examples are validated using contact between 3D solid elements. 3D solid element and 3D beam have different kinematics, so analysis result can be different. In this sub-chapter, differences between 3D solid element in ANSYS and 3D beam element are compared by examples of beam deflection.

The example is the cantilever straight beam and the tip of beam is displaced -30 along Z-axis.

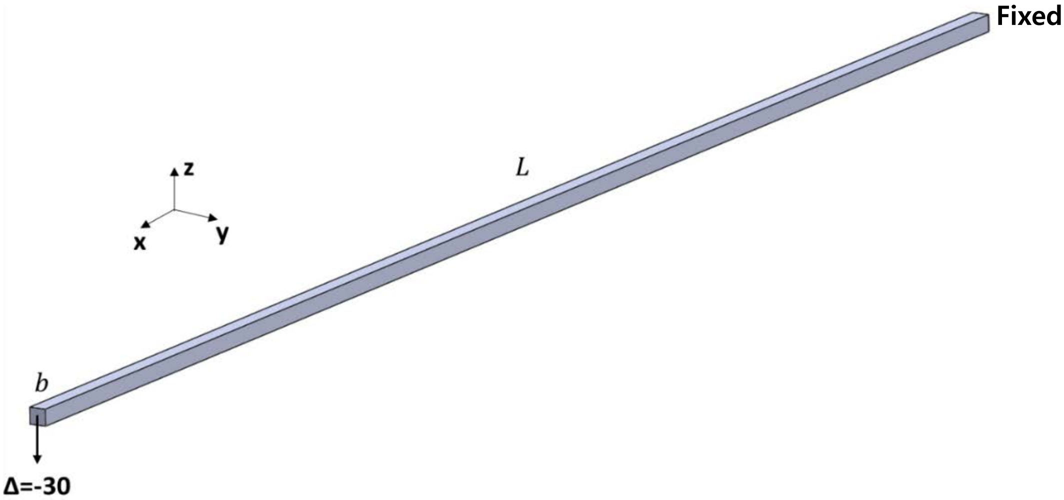

Figure 5.1 Cantilever square beam

Young's modulus E is 20×10^5 and Poisson's ratio is 0.3. The length of beam L is 100, and the thickness of square beam b is 1. Results are obtained as

Reference result of ANSYS		Result of code – 10 elements		Result of code – 100 elements	
u_x	-5.576	u_x	-5.4207	u_x	-5.4368
u_y	≈ 0	u_y	≈ 0	u_y	≈ 0
u_z	-30	u_z	-30	u_z	-30

Table 5.1 Results of cantilever square beam deflection

The displacements of z-axis direction are given value, and the displacements of y-axis direction are near zero because beam is not affected in y-axis direction due to force direction. Therefore, the displacements of x-axis direction are compared. These values have error of about 3 percent. The difference depending on the number of elements is insignificant. In the examples, there will be errors due to difference of element.

5.2 Contact between rectangular cross-section beams

The example is in paper 'Contact between 3D beams with rectangular cross-sections', Litewka and Wriggers, 2002 [4]. The configuration and properties of the example are shown in figure 5.2 and table 5.2. In the example, the cross-section of beam is rhombic (diamond shape), so contact points exist at the edge of the beams. In the paper, rectangular 3D Timoshenko beam element is used, and contact is checked as figure 4.7.

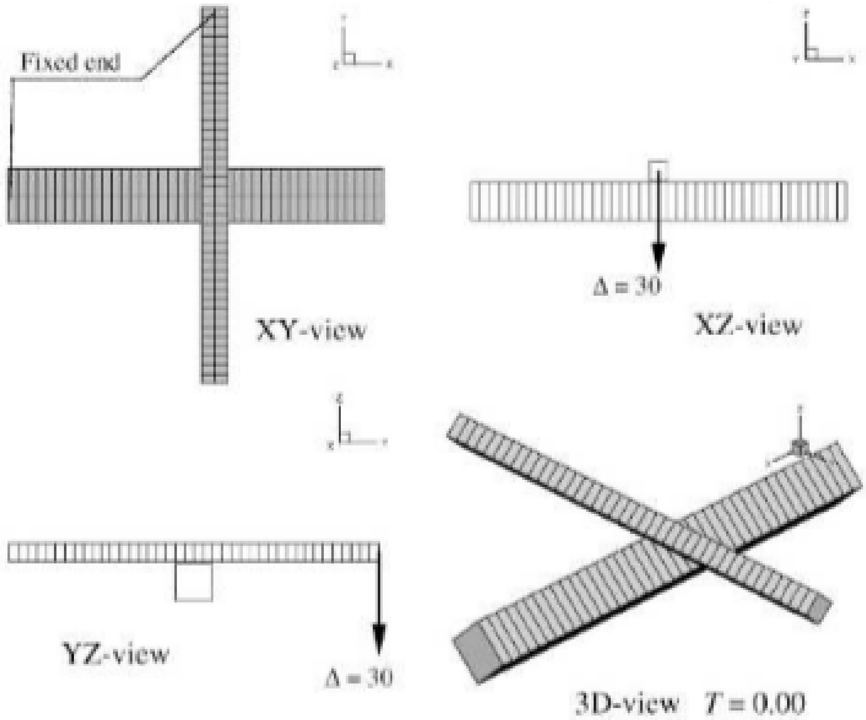

Figure 5.2 Contact between rectangular cross-section beams

Upper beam		Lower beam	
E (Young's modulus)	20×10^3	E (Young's modulus)	30×10^3
υ (Poisson's ratio)	0.3	υ (Poisson's ratio)	0.17
$b_s = b_t$	5	$b_s = b_t$	10
L	100	L	100
Initial gap		1.393	
The tip of upper beam is displaced -30 along Z-axis toward 16 elements			

Table 5.2 Properties of two rectangular cross-section beams

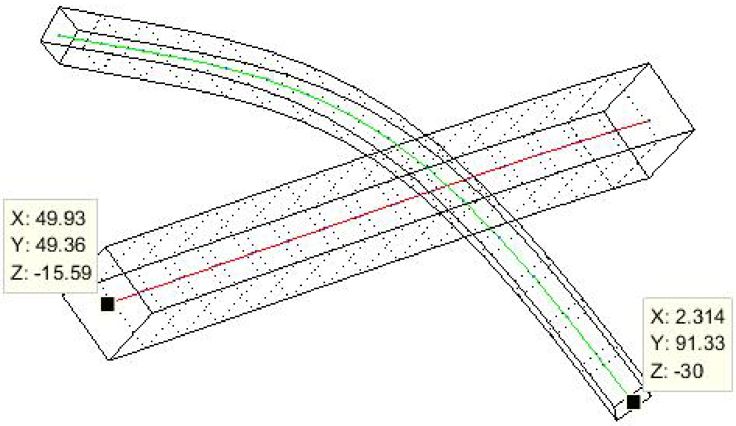

Figure 5.3 Result of contact between rectangular cross-section beams

Reference result of paper		Reference result of ANSYS		Result of code	
Upper beam		Upper beam		Upper beam	
u_x	3.261	u_x	2.1561	u_x	2.314
u_y	-8.260	u_y	-8.3781	u_y	-8.67
u_z	-30	u_z	-30	u_z	-30
Lower beam		Lower beam		Lower beam	
u_x	-0.103	u_x	-0.0968	u_x	-0.07
u_y	-1.331	u_y	-2.2207	u_y	-0.67
u_z	-4.147	u_z	-3.5772	u_z	-3.59

Table 5.3 Results of contact between rectangular cross-section beams

For the cross validation, result of ANSYS is used. In analysis of ANSYS, use fine mesh and 3D solid element contact. In the upper beam where displacement control is applied, the results show an error of between 3 and 7 percent. this error is similar to the error due to the element difference compared in 5.1. In the lower beam, which changes due to contact with the upper beam, the result is much more error than for the upper beam. In particular, the error is larger in the non-main displacement part as u_y of the lower beam. This error difference seems to be due to the difference in direction of the contact force or contact method, but the displacement results have the same order. The reference of the paper and the result of ANSYS show a similar difference. If consider difference between reference of the paper and the results of ANSYS, the results of code is an acceptable range of analysis.

5.3 Contact between beams for four plane elements in cross-section

In this example, two cantilever beams having an octagonal cross-section are used. The configuration and properties of the example are shown in figure 5.4 and table 5.4. Similar to the example in 5.2, contact points will exist at the edge of the beams, but as the beam deforms downward, the contacting edge will change.

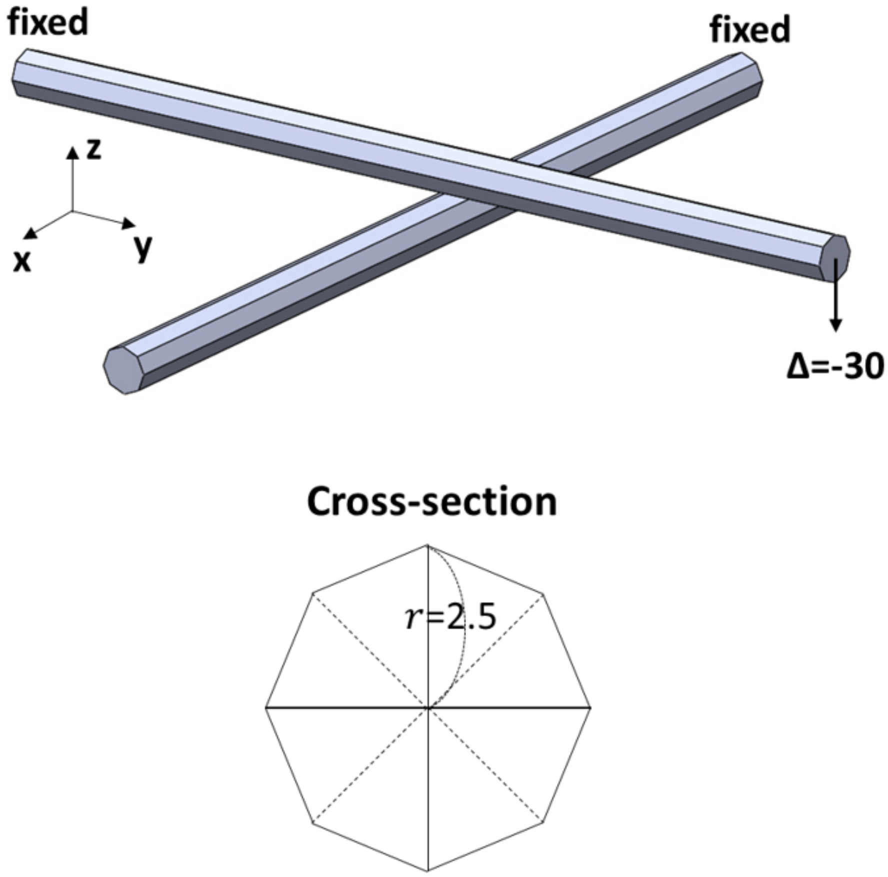

Figure 5.4 Contact between beams for four plane elements in cross-section

Beams	
E (Young's modulus)	20×10^3
υ (Poisson's ratio)	0.3
r	2.5
L	100
Initial gap	1
The tip of upper beam is displaced -30 along Z-axis toward 10 elements	

Table 5.4 Properties of two beams for four plane elements in cross-section

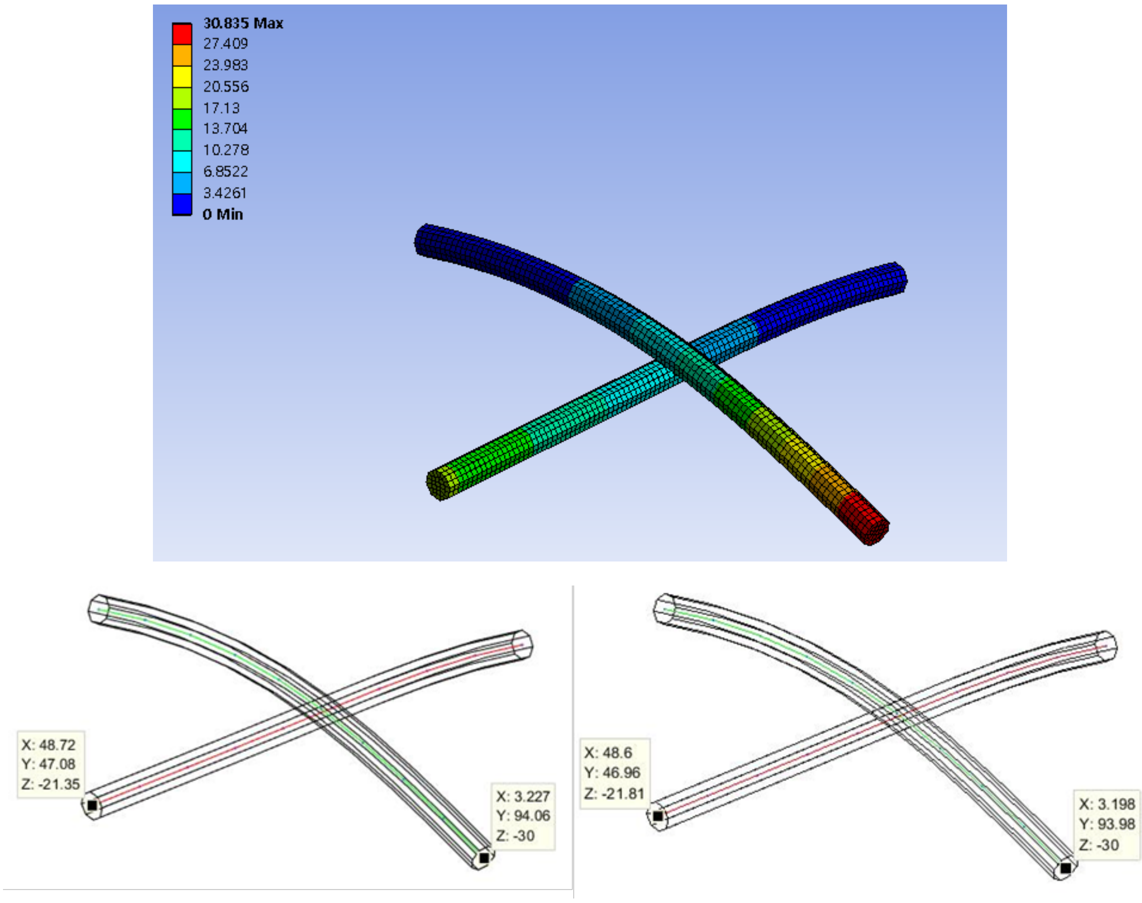

Figure 5.5 Results of contact between beams for four plane elements in cross-section

Reference result of ANSYS		Result – 40step		Result – 100step	
Upper beam		Upper beam		Upper beam	
u_x	3.1307	u_x	3.2270	u_x	3.198
u_y	-5.9954	u_y	-5.9418	u_y	-6.02
u_z	-30	u_z	-30	u_z	-30
Lower beam		Lower beam		Lower beam	
u_x	-1.7615	u_x	-1.2797	u_x	-1.40
u_y	-4.1277	u_y	-2.9222	u_y	-3.04
u_z	-17.047	u_z	-15.3463	u_z	-15.81

Table 5.5 Results of contact between beams for four plane elements in cross-section

Similar to the example in 5.2, in the upper beam where displacement control is applied, the results show errors within 2 percent, the error is similar to the error due to the element difference compared in 5.1. On the other hand, in the lower beam, which changes due to contact with the upper beam, the result is much more error than for the upper beam. In particular, the error is larger in the non-main displacement part as u_x, u_y of the lower beam. This error difference seems to be due to the difference in direction of contact force or contact method, but the displacement results have the same order in both results. In addition, the more force steps, the more converging on the result of the ANSYS reference. This is because if the displacement is larger than the elements size, an error occurs in the contact process.

5.4 Contact between square hollow rectangular beam and square beam

In this example, a cantilever beam having a hollow rectangular cross-section and a cantilever beam having a square cross-section are used. The configuration and properties of the example are shown in figure 5.6 and table 5.6. In existing beam-to-beam contact methods, there is no way to analysis beams having a cross-section of I, H and etc. In the example, as the inner beam moves to the left and up, the inner beam contact the inner surface of the hollow beam.

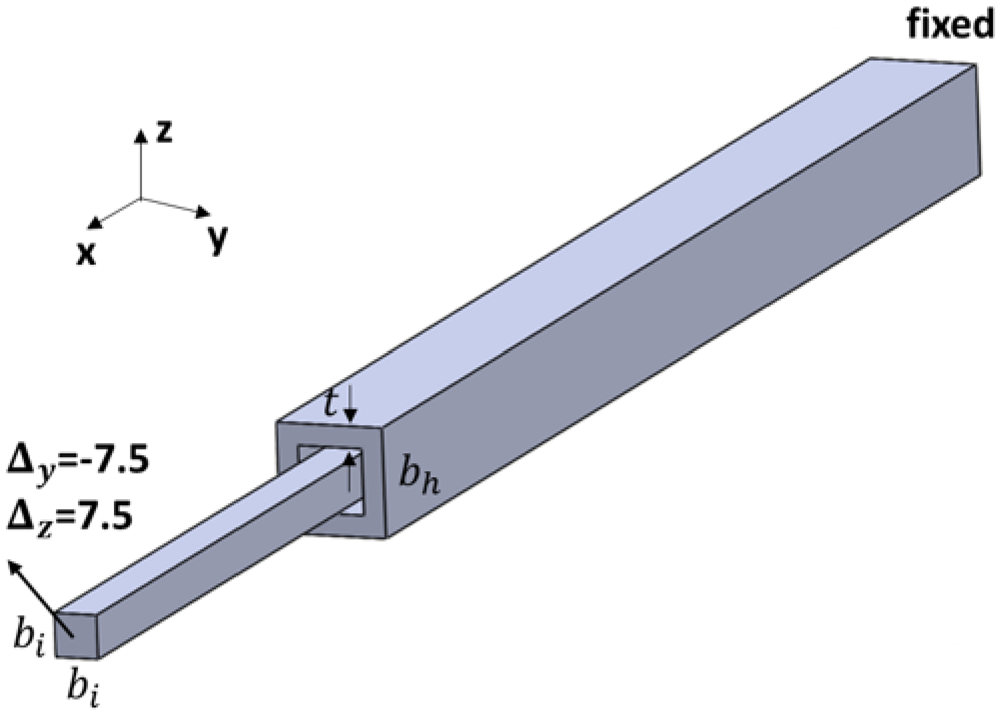

Figure 5.6 Contact between square hollow rectangular beam and square beam

Hollow beam		Inner beam	
E (Young's modulus)	20×10^3	E (Young's modulus)	20×10^5
υ (Poisson's ratio)	0.3	υ (Poisson's ratio)	0.3
t	2	b_i	2
L	70	L	100
Initial gap		2	
The tip of inner beam is displaced 7.5 along Z-axis toward displaced -7.5 along Y-axis toward 10 elements			

Table 5.6 Properties of square hollow rectangular beam and square beam

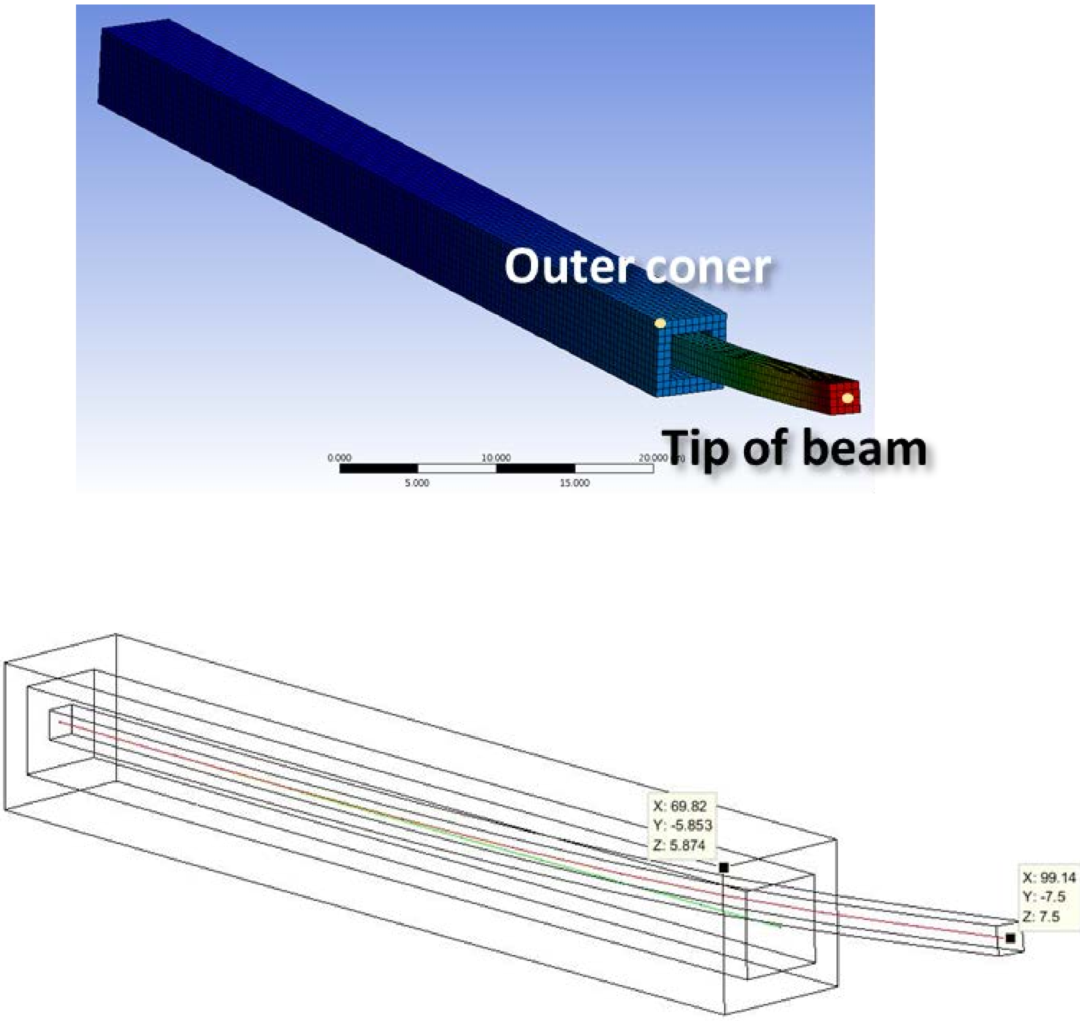

Figure 5.7 Results of contact between square hollow rectangular beam and square beam

Reference result of ANSYS		Result – 50step		Result – 100step	
Hollow beam		Hollow beam		Hollow beam	
u_x	-0.144	u_x	-0.18	u_x	-0.18
u_y	-1.126	u_y	-0.853	u_y	-0.886
u_z	1.126	u_z	0.874	u_z	0.901
Inner beam		Inner beam		Inner beam	
u_x	-1.379	u_x	-0.86	u_x	-0.9
u_y	-7.5	u_y	-7.5	u_y	-7.5
u_z	7.5	u_z	7.5	u_z	7.5

Table 5.7 Results of contact between square hollow rectangular beam and square beam

Unlike to the example in 5.2 and 5.3, both the inner beam and the hollow beam have relatively large errors than the error due to the element difference. The difference from the previous examples is that this example uses parallel beams. Parallel beams can have an error when it is solved as the point-to-point contact method because the multiple contact points can exist along the longitudinal direction of beam [6]. In the results, the hollow beam has a larger displacement in the longitudinal direction than the reference, the inner beam has a smaller displacement in the longitudinal direction than the reference. This seems to be the result of pushing in the longitudinal direction because a concentrated load is applied at one contact point. As the hollow beam is pressed in the longitudinal direction, the displacement in the cross-sectional direction is relatively small. However, the displacement results still have the same order in both results. It can be confirmed that the beam of the shape, which cannot be analyzed previously, can be solved as an order similar to that of a commercial software. In addition, the more force steps, the more converging on the result of the ANSYS reference. This is because if the displacement is larger than the elements size, an error occurs in the contact process.

Chapter 6. Conclusions

In this paper, suggest modeling of beam-to-beam contact method with arbitrary cross-sections. For contact method, 3D beam elements with arbitrary cross-sections are used. 3D beam elements are made based on 3D solid elements and degeneration of solid elements. These elements have information of cross-section in beam node. And these elements have warping degree of freedom.

Point-to-point contact method is widely used beam contact method. This formulation searches closest points using orthogonality conditions. Most of applied papers about beam-to-beam contact are based point-to-point contact. Based on point-to-point contact, multiple-point contact between beams was also developed. But point-to-point contact method was developed on the basis of circular cross-section beams. beam-to-beam contact with rectangular cross-sections is suggested, but that method can't use for arbitrary cross sections such as I beam, L beam and even arbitrary quadrilateral cross-section.

For simulate beam contact with arbitrary cross-sections, contact formulation based on point-to-point contact is modified. First, closest surface points are searched. For efficient searching of closest points, search step is divided into two parts, global search and local search, and determination of contact possibility is performed in local search. To the next, contact formulation is performed along surface line of beam similar to point-to-point contact. Finally, validation was performed through several examples. The results are converged with the results of 3D solid elements in commercial software, and the results are shown that can solve examples where existing beam-to-beam contact methods cannot be solved.

Bibliography

[1] T.R.J. Hughes, R.L. Taylor, J.L. Sackman, W. Kanoknukulchai, *finite element formulation and solution of contact-impact problems in continuum mechanics - IV*, Report no. UC SESM 76-4, July 1976

[2] P. Wriggers, G. Zavarise, *On contact between three-dimensional beams undergoing large deflections*, Communications in Numerical Methods in Engineering, Vol.13, 429-438, 1997.

[3] A.G. Neto, P. M. Pimenta, P. Wriggers, *Self-contact modeling on beams experiencing loop formation,* Computational Mechanics, Vol.55, Issue 1, pp. 193-208, January 2015

[4] P. Litewka, P. Wriggers, *Contact between 3D beams with rectangular cross-sections, International Journal for Numerical Methods in Engineering,* 53:2019-2041, 2002

[5] P. Litewka, *Frictional beam-to-beam multiple-point contact finite element*, Computational Mechanics, Vol. 56, Issue 2, pp. 243-264, August 2015

[6] C. Meier, Alexander Popp, W. A. Wall, *A finite element approach for the line-to-line contact interaction of thin beams with arbitrary orientation*, Comput. Methods Appl. Mech. Engrg. 308, pp. 377-413, 2016

[7] C. Meier, W. A. Wall, Alexander Popp, *A unified approach for beam-to-beam contact*, Comput. Methods Appl. Mech. Engrg. 315, pp. 972-1010, 2017

[8] A.G. Neto, P. M. Pimenta, P. Wriggers, *A master-surface to master-surface formulation for beam to beam contact. Part I: frictionless interaction*, Comput. Methods Appl. Mech. Engrg. 303, pp. 400-429, 2016

[9] K. Yoon, Y. Lee, PS Lee, *A continuum mechanics based 3-D beam finite element with warping displacements and its modeling capabilities*, Structural Engineering and Mechanics, Vol. 43, No. 4, pp. 411-437, 2012

[10] K. J. BATHE, *Finite element procedures*, New York, Prentice Hall, 1996

[11] John Argyris, *An excursion into large rotations*, Computer Methods in Applied Mechanics and Engineering, Vol. 32, pp. 85-155, 1982

[12] M. Ritto-Corrêa, D. Camotim, *On the differentiation of the Rodrigues formula and its significance for the vector-like parameterization of Reissner-Simo beam theory,* International Journal for Numerical Methods in Engineering, Vol.55, pp. 1005-1032, 2002

[13] G. Zavarise, Laura De Lorenzis, *The node-to-segment algorithm for 2D frictionless contact: Classical formulation and special cases, Comput*. Methods Appl. Mech. Engrg., 198, 3428-3451, 2009

[14] Eduardo N. Dvorkin, Eugenio Onate, Javier Oliver, *On a non-linear formulation for curved Timoshenko beam elements considering large displacement/rotation increments*, International Journal for Numerical Methods in Engineering, Vol. 26, 1597-1613, 1988

[15] K. Yoon, Y. Lee, PS Lee, *Nonlinear performance of continuum mechanics based beam elements focusing on large twisting behaviors*, Comput. Methods Appl. Mech. Engrg. 281, pp. 106-130, 2014

[16] D. P. Boso, B. A. Schrefler, P. Litewka, P. Wriggers, *Thermo-electro-mechanical coupling in beam-to-beam contact*, Europeam Conference on Computational Mechanics, pp. 306-306, 2008